Geometric somersaults of a polymer chain through cyclic twisting motions

Tomohiro Yanao* and Taiko Hino
Department of Applied Mechanics and Aerospace Engineering, Waseda University, Tokyo 169-8555, Japan
(Received 1 August 2016; published 23 January 2017)

This study explores the significance of geometric angle shifts, which we call geometric somersaults, arising from cyclic twisting motions of a polymer chain. A five-bead polymer chain serves as a concise and minimal model of a molecular shaft throughout this study. We first show that this polymer chain can change its orientation about its longitudinal axis largely, e.g., 120°, under conditions of zero total angular momentum by changing the two dihedral angles in a cyclic manner. This phenomenon is an example of the so-called "falling cat" phenomenon, where a falling cat undergoes a geometric somersault by changing its body shape under conditions of zero total angular momentum. We then extend the geometric somersault of the polymer chain to a noisy and viscous environment, where the polymer chain is steered by external driving forces. This extension shows that the polymer chain can achieve an orientation change keeping its total angular momentum and total external torque fluctuating around zero in a noisy and viscous environment. As an application, we argue that the geometric somersault of the polymer chain by 120° may serve as a prototypical and coarse-grained model for the rotary motion of the central shaft of ATP synthase (F_OF_1-ATPase). This geometric somersault is in clear contrast to the standard picture for the rotary motion of the central shaft as a rigid body, which generally incurs nonzero total angular momentum and nonzero total external torque. The power profile of the geometric somersault implies a preliminary mechanism for elastic power transmission. The results of this study may be of fundamental interest in twisting and rotary motions of biomolecules.

DOI: 10.1103/PhysRevE.95.012409

I. INTRODUCTION

Rotary motions play important roles in biological functions of molecular motors. Examples include the rotary motions of the central shaft of ATP synthase [1–5] and those of flagellar filaments driven by flagellar motors [6–9]. Molecular motors generally consist of protein subunits that are relatively flexible in comparison to their mechanical loads and thermal noise, yet their functions are highly robust and efficient [10–12]. Hence, the mechanisms for the rotary motions of molecular motors could be very different from the rotations of rigid bodies that we generally expect for macroscopic man-made motors.

This study is concerned with a possible mechanism through which biomolecules exploit their flexibility in achieving rotary motions. Specifically, we focus on the kinematic coupling between shape deformations and rotary motions of a polymer chain. Using such kinematic coupling, a polymer chain can indeed change its orientation even under conditions of zero total angular momentum. This is known as the so-called "falling cat" phenomenon, where a falling cat, starting from an upside-down attitude, can change its orientation in the air and is able to land on the ground with its legs down [13,14]. Throughout this process, the total angular momentum of the cat is essentially zero. This phenomenon implies that shape deformations alone are enough to induce an orientation change without causing total angular momentum or total external torque.

In the literature of molecular vibrations, the falling cat phenomenon is associated with the coupling between vibrations and rotations or the Coriolis coupling [15]. This coupling is indeed often disregarded approximately based on the so-called Eckart conditions [16–18]. Examples include normal-mode analysis of polyatomic molecules [19], clusters [20], and proteins [21–23], the method of reaction-path Hamiltonian [24,25], constrained simulations of peptides [26–28], and principal-component analysis of proteins [29,30]. While the approximate separation of vibrations and rotations is effective for small amplitude motions of molecules, the coupling between vibrations and rotations may have non-negligible effect in large-amplitude motions. Rather, such coupling could play active roles in the functions of biomolecules, as in the somersault of a falling cat.

The geometric framework for describing the falling cat phenomenon has been developed for the past few decades [31–35]. Guichardet [36], Tachibana and Iwai [37], and Iwai [38] developed a geometric setting for describing the coupling between vibrations and rotations in polyatomic molecules. Littlejohn and Reinsch [39] formulated the gauge fields responsible for this coupling in the n-body problem. Dynamical roles of the gauge fields and associated non-Euclidean geometry have been explored in structural transitions of small clusters and molecules in vacuum [40–44] and in a random environment [45]. Moreover, mathematically similar gauge fields arise in the swimming of microorganisms at low Reynolds numbers [46–48], in the swimming in curved space-time [49], in robotic locomotion [50–53], and in the locomotion in granular media [54]. Given the recent progress in these geometric methods, it is of fundamental interest to explore the roles of the gauge fields responsible for the coupling between shape deformations and rotary motions in biological functions of molecular motors. Although one can hardly expect that the total angular momentum of a biomolecule is conserved to zero in the noisy and viscous environment, it may still be possible that the total angular momentum is kept fluctuating around zero. In such a situation, the gauge fields responsible for the coupling between vibrations and rotations could play a dominant role.

*Author to whom correspondence should be addressed: yanao@waseda.jp

Among molecular motors, F_OF_1-ATPase has been attracting significant interest as a ubiquitous and conserved rotary motor in biological systems [1–5]. This motor consists mainly of two domains, the membrane-embedded F_O domain and water-soluble F_1 domain. These two domains are connected with a central rotary shaft. The F_O and F_1 domains drive the rotary motions of the central shaft in opposite directions, which are associated with reverse functions: Hydrolysis of ATP in the F_1 domain induces a stepwise rotary motion of the central shaft by 120° in a counterclockwise manner (when observed from the membrane side), which is in turn supposed to transmit energy to the F_O domain to translocate protons [55]. This stepwise rotary motion by 120° is known to consist of two substeps [5,56,57]. On the other hand, proton-motive force at F_O domain induces a rotary motion of the central shaft in a clockwise manner (when observed from the membrane side) [55,58–60], which is in turn supposed to transmit energy to the F_1 domain to synthesize ATP [61].

The rotary motion of the central shaft may generally suggest a "rigid-body rotation," in which the effect of shape deformation is negligible and the rotary motion is characterized by a single angular variable about a single axis. However, recent studies have indicated possible difficulties with the rigid-body rotation and rather indicated the significance of twist deformations of the central shaft: For one thing, the mismatch between the rotational symmetries of F_O and F_1 domains suggests the need for the mechanism of an elastic power transmission between these two domains [55,60,62–64], in which the central shaft twists and stores energy temporarily to smooth out the movement of the motor. Based on this indication, recent experiments [62,63] and atomistic numerical simulations [64] identified torsionally compliant parts of the central shaft. For another, since the central shaft is intrinsically bent and is situated in a narrow cavity of the molecular motor, a rigid-body rotation of the central shaft may face severe steric hindrances due to the surrounding subunits. Thus, Kutzner *et al.* [65] introduced a novel simulation method of flexible axis rotation, where the central shaft is subdivided into rotary slabs and adopts to steric restraints flexibly like a "flexible pipe cleaner." They showed that the flexible axis rotation of the central shaft requires less amount of total torque and mechanical work than the rigid-body rotation in the narrow cavity of molecular motor.

In this study, we highlight the kinematic coupling between twisting motions and rotations of a five-bead polymer chain, with the expectation that such coupling might play an essential role in the rotary motions of the central shaft of F_OF_1-ATPase. We first show that a cyclic twisting motion of the five-bead polymer chain can give rise to a stepwise angle shift by 120° about its longitudinal axis under conditions of zero total angular momentum. This is a manifestation of the falling cat phenomenon, and we call it a *geometric somersault* of the polymer chain. We then extend this geometric somersault to a noisy and viscous environment using the Langevin dynamics, where the polymer chain is steered by external forces and achieves an angle shift by 120° with keeping total angular momentum and total external torque fluctuating around zero. This is in clear contrast to the rigid-body rotation of the polymer chain, which inevitably incurs nonzero total angular momentum and nonzero total external torque. We finally discuss the relevance of the geometric somersault of the five-bead polymer chain as a prototypical model of the rotary motion of the central shaft of the F_OF_1-ATPase. The model suggests a preliminary mechanism for the elastic power transmission, where the polymer chain temporarily stores and accumulates the input energy in the form of twisting potential energy and releases it later.

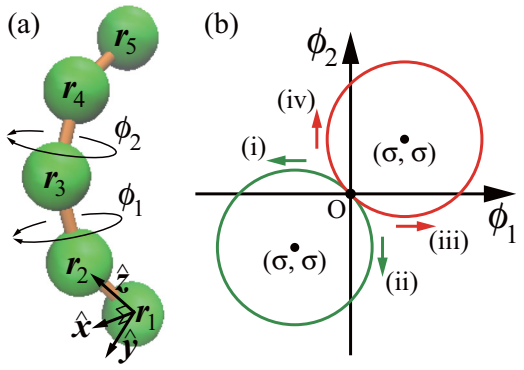

FIG. 1. (a) Schematic illustration of the five-bead polymer chain. This chain consists of five mass points, i.e., beads, of equal mass connected with four bonds. The chain has three bending angles θ_1, θ_2, and θ_3 and two dihedral angles ϕ_1 and ϕ_2. The body-fixed frame $\mathsf{R} \equiv (\hat{x},\hat{y},\hat{z})$ is located at the first bead. (b) Four typical cyclic paths of interest in this study, paths (i)–(iv), in the space of dihedral angles ϕ_1 and ϕ_2. All the four paths are circular in the space of dihedral angles, starting from and returning to the origin $(\phi_1,\phi_2) = (0°,0°)$, representing cyclic twisting motions of the five-bead polymer chain. These paths are parametrized by Eqs. (26) and (27), where σ determines the center and the radius of the circular paths. Typical values of σ in this study are $\sigma = -70.88°$ for paths (i) and (ii), and $\sigma = 70.88°$ for paths (iii) and (iv).

This paper is organized as follows. In Sec. II, we present a gauge-theoretical framework for the computation of geometric somersault of the five-bead polymer chain in vacuum. Section III extends the geometric somersault to a noisy and viscous environment using the Langevin dynamics, and compares it with a rigid-body rotation of the five-bead polymer chain. We finally discuss implications of the geometric somersault of the five-bead polymer chain for the rotary motion of the central shaft of F_OF_1-ATPase. Section IV concludes this paper with some remarks on future studies.

II. GEOMETRIC SOMERSAULTS OF A FIVE-BEAD POLYMER CHAIN IN VACUUM

This section scrutinizes the geometric angle shifts, i.e., geometric somersaults, arising from torsional kinematics of a five-bead polymer chain in vacuum. We show that a cyclic twisting motion of the five-bead polymer chain can give rise to a geometric angle shift by 120° about its longitudinal axis under conditions of zero total angular momentum.

A. Model and coordinates

A five-bead polymer chain serves as a concise model of a molecular shaft throughout this study. Configuration of this model is shown in Fig. 1(a). This model consists of five

mass points, i.e., beads, of equal mass, $m_i = m$ ($i = 1,\ldots,5$), connected with four bonds. In the present section (Sec. II), the length of the four bonds is fixed to a. Thus, the shape of the five-bead polymer chain is parametrized by three bending angles θ_1, θ_2, and θ_3, and two dihedral angles, ϕ_1 and ϕ_2, in the following manner [66,67].

We first introduce a body-fixed frame, which specifies instantaneous orientation of the system. The body-fixed frame is represented by a three-dimensional orthogonal matrix $\mathsf{R} \in \mathrm{SO}(3)$, whose three columns consist of a triplet of orthogonal unit vectors $\mathsf{R} \equiv (\hat{\boldsymbol{x}},\hat{\boldsymbol{y}},\hat{\boldsymbol{z}})$ [see Fig. 1(a)]. Let the position of ith ($i = 1,\ldots,5$) bead with respect to the body-fixed frame be represented by the three-dimensional vector $\boldsymbol{r}_i = (x_i,y_i,z_i)^T$. We assume that the origin of the body-fixed frame coincides with the first bead. Thus, $\boldsymbol{r}_1 = (0,0,0)^T$. The $\hat{\boldsymbol{z}}$ axis of the body-fixed frame R is set parallel to the vector connecting the first and the second beads $\boldsymbol{r}_2 - \boldsymbol{r}_1$. The $\hat{\boldsymbol{y}}$ axis is defined to be perpendicular to the $\hat{\boldsymbol{z}}$ axis and to lie within the plane spanned by the first three beads at $\boldsymbol{r}_1$, $\boldsymbol{r}_2$, and $\boldsymbol{r}_3$. The $\hat{\boldsymbol{x}}$ axis is defined as $\hat{\boldsymbol{x}} = \hat{\boldsymbol{y}} \times \hat{\boldsymbol{z}}$. Thus, the position of the second bead with respect to the body-fixed frame R is represented by $\boldsymbol{r}_2 = (0,0,a)^T$. Hereafter, T on a vector or a matrix represents the transposition.

The positions of the third, fourth, and fifth beads, $\boldsymbol{r}_3$, $\boldsymbol{r}_4$, and $\boldsymbol{r}_5$, are represented as

$$\boldsymbol{r}_3 = \boldsymbol{r}_2 + \mathsf{R}_3^2(0^\circ,\theta_1)\boldsymbol{a}, \tag{1}$$

$$\boldsymbol{r}_4 = \boldsymbol{r}_3 + \mathsf{R}_3^2(0^\circ,\theta_1)\mathsf{R}_4^3(\phi_1,\theta_2)\boldsymbol{a}, \tag{2}$$

$$\boldsymbol{r}_5 = \boldsymbol{r}_4 + \mathsf{R}_3^2(0^\circ,\theta_1)\mathsf{R}_4^3(\phi_1,\theta_2)\mathsf{R}_5^4(\phi_2,\theta_3)\boldsymbol{a}, \tag{3}$$

where we have introduced the matrices

$$\mathsf{R}_i^{i-1}(\phi_{i-3},\theta_{i-2}) \equiv \begin{pmatrix} \cos\phi_{i-3} & -\sin\phi_{i-3} & 0 \\ \sin\phi_{i-3} & \cos\phi_{i-3} & 0 \\ 0 & 0 & 1 \end{pmatrix} \times \begin{pmatrix} 1 & 0 & 0 \\ 0 & \cos\theta_{i-2} & -\sin\theta_{i-2} \\ 0 & \sin\theta_{i-2} & \cos\theta_{i-2} \end{pmatrix} \quad (i = 3,4,5), \tag{4}$$

with $\phi_0 \equiv 0^\circ$, and a vector $\boldsymbol{a} \equiv (0,0,a)^T$. Note that θ_i ($i = 1,2,3$) is the bending angle of the polymer chain at $(i+1)$th bead, and ϕ_i ($i = 1,2$) is the dihedral angle between the planes spanned by the three beads at $\{\boldsymbol{r}_i,\boldsymbol{r}_{i+1},\boldsymbol{r}_{i+2}\}$ and at $\{\boldsymbol{r}_{i+1},\boldsymbol{r}_{i+2},\boldsymbol{r}_{i+3}\}$. In this study, we assume that the ranges of these angles are

$$0^\circ \leqslant \theta_i < 180^\circ \quad (i = 1,2,3), \tag{5}$$

$$-180^\circ \leqslant \phi_i < 180^\circ \quad (i = 1,2). \tag{6}$$

A positive value of ϕ_i characterizes a right-handed twist, while a negative value of ϕ_i characterizes a left-handed twist.

In the present section (Sec. II), we fix all the bending angles to $\theta_1 = \theta_2 = \theta_3 = 30^\circ$, in order to reduce the degree of freedom for simplicity and to focus on the torsional kinematics of the model. The reason for the nonzero bending angles is that the central shaft of the ATP synthase ($\mathrm{F_OF_1}$-ATPase) is intrinsically bent [2,64]. In addition, it is necessary to avoid zero bending angles in order to define the dihedral angles uniquely. Thus, only the two dihedral angles, ϕ_1 and ϕ_2, determine the shape of the system uniquely in Sec. II.

It is convenient to introduce a two-dimensional space of ϕ_1 and ϕ_2 as shown in Fig. 1(b). This two-dimensional space of dihedral angles serves as a *shape space* in the sense that a point in this space specifies the shape of the five-bead polymer chain uniquely. A closed path in this shape space represents a *cyclic twisting motion* of the system. Figure 1(b) shows four typical cyclic paths of interest in this study, (i)–(iv). All the four paths are circular in the space of dihedral angles, starting from and returning to the origin, $(\phi_1,\phi_2) = (0^\circ,0^\circ)$, which corresponds to the planar and uniformly bent conformation of the polymer chain as shown in Fig. 1(a). The parameter σ determines the center and the radius of the circular paths. Paths (i) and (ii) follow the same circular orbit in opposite directions. Paths (iii) and (iv) follow as well. In the following subsections, we consider geometric angle shifts of the polymer chain arising from the cyclic twisting motions represented by these paths.

B. Gauge-theoretical description of the coupling between twisting motions and rotations

This section describes the geometric angle shifts of the five-bead polymer chain, which are characterized by the movements of the body-fixed frame R, arising from twisting motions due to dihedral angles ϕ_1 and ϕ_2 under conditions of zero total angular momentum. See Ref. [39] for more general and systematic account for the gauge fields responsible for the coupling between internal motions and rotations.

We denote the position of ith bead of the polymer chain with respect to the space-fixed frame by a three-dimensional column vector $\boldsymbol{r}_{si} = (x_{si},y_{si},z_{si})^T$ ($i = 1,\ldots,5$). The subscript s of $\boldsymbol{r}_{si}$ indicates the vector with respect to the space-fixed frame, whereas the vector $\boldsymbol{r}_i$ without the subscript s, such as the one appeared in Sec. II A, represents the position vector with respect to the body-fixed frame R. Hereafter, we adopt a similar convention for the subscript s, indicating a variable with respect to the space-fixed frame [39]. The relation between $\boldsymbol{r}_{si}$ and $\boldsymbol{r}_i$ is

$$\boldsymbol{r}_{si} - \boldsymbol{c}_s = \mathsf{R}(\boldsymbol{r}_i - \boldsymbol{c}) \quad (i = 1,\ldots,5), \tag{7}$$

where

$$\boldsymbol{c}_s = \frac{\sum_{i=1}^5 m_i \boldsymbol{r}_{si}}{\sum_{i=1}^5 m_i}, \quad \boldsymbol{c} = \frac{\sum_{i=1}^5 m_i \boldsymbol{r}_i}{\sum_{i=1}^5 m_i}. \tag{8}$$

The vector $\boldsymbol{c}_s$ represents the center of mass of the system with respect to the space-fixed frame, while the vector $\boldsymbol{c}$ represents the center of mass of the system with respect to the body-fixed frame. Throughout Sec. II, we assume that the total linear momentum of the polymer chain is conserved to zero, assuming that the system is in vacuum and is isolated. Thus, $\boldsymbol{c}_s$ is independent of time and can be set to the origin of the space-fixed frame, i.e., $\boldsymbol{c}_s = \boldsymbol{0}$, without loss of generality.

In order to separate the translational degrees of freedom from the overall system, we employ the mass-weighted Jacobi coordinates with respect to the space-fixed frame $\{\boldsymbol{\rho}_{si}\}$, which

are defined as [68]

$$\boldsymbol{\rho}_{si} = \sqrt{\mu_i}\left(\frac{\sum_{k=1}^{i} m_k \boldsymbol{r}_{sk}}{\sum_{k=1}^{i} m_k} - \boldsymbol{r}_{s,i+1}\right) \quad (i = 1,\ldots,4), \tag{9}$$

where μ_i are the reduced masses defined by

$$\mu_i = \frac{m_{i+1}\sum_{k=1}^{i} m_k}{\sum_{k=1}^{i+1} m_k} \quad (i = 1,\ldots,4). \tag{10}$$

The mass-weighted Jacobi coordinates with respect to the body-fixed frame $\{\boldsymbol{\rho}_i\}$ are determined from $\{\boldsymbol{r}_i\}$ in the same manner as Eq. (9), and are related to $\{\boldsymbol{\rho}_{si}\}$ in a similar manner to Eq. (7):

$$\boldsymbol{\rho}_{si} = \mathsf{R}\boldsymbol{\rho}_i(\phi_1,\phi_2) \quad (i = 1,\ldots,4). \tag{11}$$

Note that $\{\boldsymbol{\rho}_i\}$ are the functions of only dihedral angles ϕ_1 and ϕ_2 since all the bending angles are assumed to be constant as noted in Sec. II A, while $\{\boldsymbol{\rho}_{si}\}$ depend on both the dihedral angles ϕ_1 and ϕ_2 and the body-fixed frame R.

Differentiation of Eq. (11) with respect to time gives

$$\dot{\boldsymbol{\rho}}_{si} = \dot{\mathsf{R}}\boldsymbol{\rho}_i + \mathsf{R}\sum_{\mu=1}^{2}\frac{\partial \boldsymbol{\rho}_i}{\partial \phi_\mu}\dot{\phi}_\mu. \tag{12}$$

Hereafter, a dot over a variable represents the time derivative. Total angular momentum of the system with respect to the space-fixed frame $\boldsymbol{L}_s$ is

$$\boldsymbol{L}_s = \sum_{i=1}^{4}\boldsymbol{\rho}_{si}\times\dot{\boldsymbol{\rho}}_{si}. \tag{13}$$

Using Eqs. (11) and (12), total angular momentum with respect to the body-fixed frame $\boldsymbol{L} = \mathsf{R}^T\boldsymbol{L}_s$ is written as

$$\boldsymbol{L} = \sum_{i=1}^{4}\boldsymbol{\rho}_i\times(\boldsymbol{\omega}\times\boldsymbol{\rho}_i) + \sum_{\mu=1}^{2}\sum_{i=1}^{4}\boldsymbol{\rho}_i\times\frac{\partial\boldsymbol{\rho}_i}{\partial\phi_\mu}\dot{\phi}^\mu, \tag{14}$$

where $\boldsymbol{\omega}$ is the angular velocity vector of the body-fixed frame with respect to the body-fixed frame itself. The three-dimensional vector $\boldsymbol{\omega}$ is related to the angular velocity matrix Ω as

$$\Omega \equiv \mathsf{R}^T\dot{\mathsf{R}} = \begin{pmatrix} 0 & -\omega_z & \omega_y \\ \omega_z & 0 & -\omega_x \\ -\omega_y & \omega_x & 0 \end{pmatrix} \Leftrightarrow \boldsymbol{\omega} \equiv \begin{pmatrix}\omega_x\\ \omega_y\\ \omega_z\end{pmatrix}. \tag{15}$$

Equation (14) can be written more compactly as

$$\boldsymbol{L} = \mathsf{M}\left(\boldsymbol{\omega} + \sum_{\mu=1}^{2}\boldsymbol{A}_\mu\dot{\phi}_\mu\right), \tag{16}$$

where M is the moment-of-inertia tensor with respect to the body-fixed frame, whose components are

$$M_{\alpha\beta} = \sum_{i=1}^{4}[(\boldsymbol{\rho}_i\cdot\boldsymbol{\rho}_i)\delta_{\alpha\beta} - \rho_{i\alpha}\rho_{i\beta}], \tag{17}$$

where α and β specify the axes of the body-fixed frame ($\alpha,\beta = x,y,z$), and $\delta_{\alpha\beta}$ is the Kronecker delta. $\boldsymbol{A}_\mu$ in Eq. (16) is the gauge potential [39] defined by

$$\boldsymbol{A}_\mu = \mathsf{M}^{-1}\left(\sum_{i=1}^{4}\boldsymbol{\rho}_i\times\frac{\partial\boldsymbol{\rho}_i}{\partial\phi_\mu}\right). \tag{18}$$

The corresponding curvature form, which is also referred to as Coriolis tensor [39], is given by

$$\boldsymbol{B}_{\mu\nu} = \frac{\partial\boldsymbol{A}_\nu}{\partial\phi_\mu} - \frac{\partial\boldsymbol{A}_\mu}{\partial\phi_\nu} - \boldsymbol{A}_\mu\times\boldsymbol{A}_\nu. \tag{19}$$

Under conditions of zero total angular momentum, $\boldsymbol{L}_s = \boldsymbol{L} = \boldsymbol{0}$, Eq. (16) reduces to

$$\boldsymbol{\omega} = -\boldsymbol{A}_1\dot{\phi}_1 - \boldsymbol{A}_2\dot{\phi}_2. \tag{20}$$

This equation determines the instantaneous angular velocity of the body-fixed frame $\boldsymbol{\omega}$ arising from the movements of dihedral angles $\dot{\phi}_1$ and $\dot{\phi}_2$ under conditions of zero total angular momentum. That is, for a given time evolution of $\dot{\phi}_1(t)$ and $\dot{\phi}_2(t)$, Eq. (20) determines the corresponding evolution of $\boldsymbol{\omega}(t)$ and its matrix representation $\Omega(t)$ [see Eq. (15)] under conditions of zero total angular momentum. Using this $\Omega(t)$, one can compute the movement of the body-fixed frame under conditions of zero total angular momentum by solving the differential equation

$$\dot{\mathsf{R}} = \mathsf{R}\Omega(t). \tag{21}$$

The solution of Eq. (21) is expressed as a time- or path-ordered product as

$$\mathsf{R}(t) = \mathsf{R}_0 T\exp\left[\int_0^t \Omega(s)ds\right] \tag{22}$$

$$= \mathsf{R}_0 P\exp\left[\int_C(-\mathsf{A}_1 d\phi_1 - \mathsf{A}_2 d\phi_2)\right], \tag{23}$$

where R_0 is the initial body-fixed frame, and T and P represent time and path orderings. In Eq. (23), C on the integral sign represents a path in the space of dihedral angles such as the one in Fig. 1(b), and A_1 and A_2 are the matrix representations of $\boldsymbol{A}_1$ and $\boldsymbol{A}_2$. The relation between $\boldsymbol{A}_i$ and A_i ($i = 1,2$) is the same as the one between $\boldsymbol{\omega}$ and Ω in Eq. (15).

In this study, we compute the movements of the body-fixed frame R using quaternions [69], instead of solving Eq. (21) directly. Using quaternions (q_0,q_1,q_2,q_3), one can express the transpose of the body-fixed frame R^T as

$$\mathsf{R}^T = \begin{pmatrix} q_0^2+q_1^2-q_2^2-q_3^2 & 2(q_1q_2+q_0q_3) & 2(q_1q_3-q_0q_2) \\ 2(q_1q_2-q_0q_3) & q_0^2-q_1^2+q_2^2-q_3^2 & 2(q_2q_3+q_0q_1) \\ 2(q_1q_3+q_0q_2) & 2(q_2q_3-q_0q_1) & q_0^2-q_1^2-q_2^2+q_3^2 \end{pmatrix}. \tag{24}$$

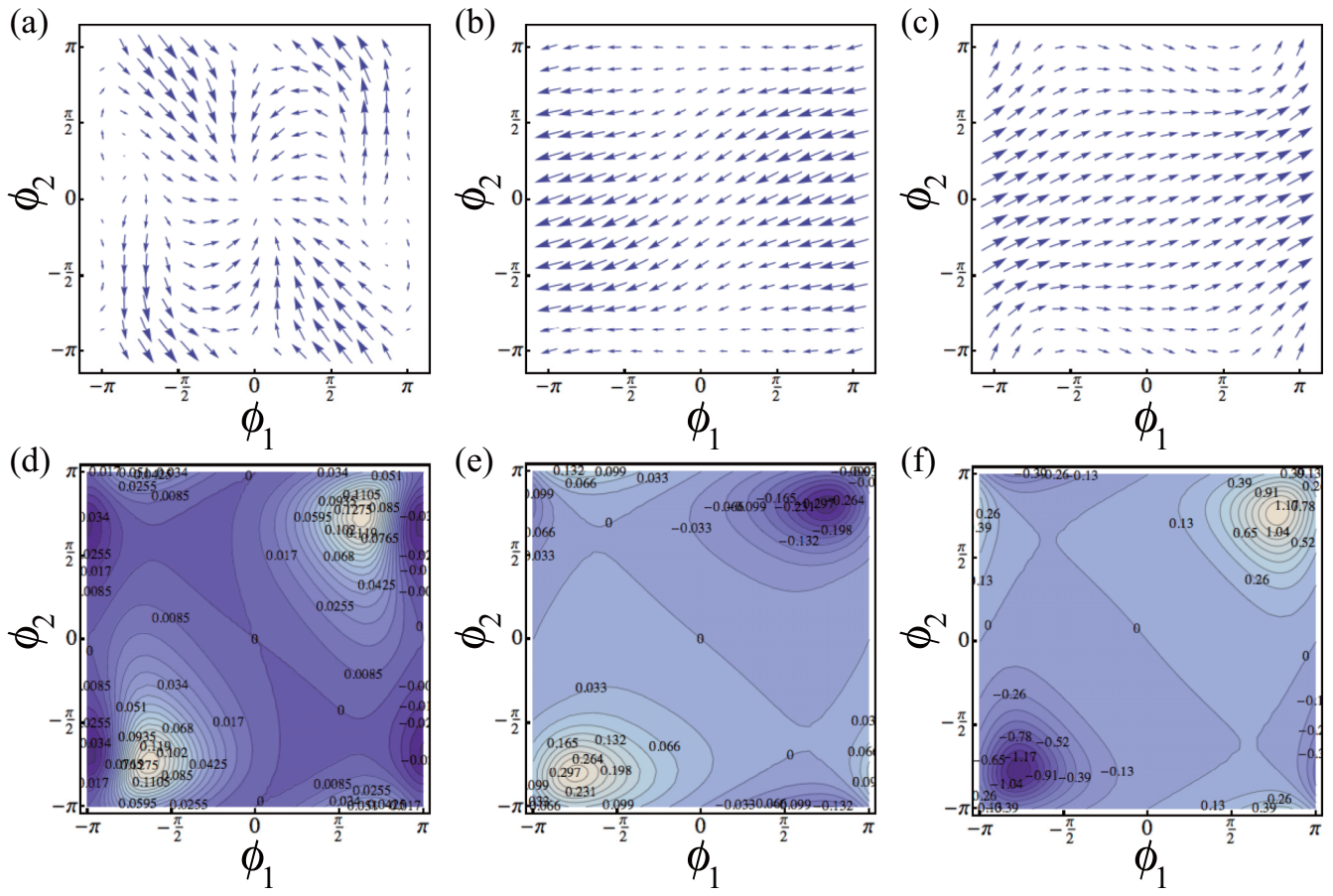

FIG. 2. Upper three panels show the fields of the gauge potentials of the five-bead polymer chain (a) $\boldsymbol{A}_x$, (b) $\boldsymbol{A}_y$, and (c) $\boldsymbol{A}_z$ in the space of two dihedral angles ϕ_1 and ϕ_2. Lower three panels show the contour plots of the corresponding components of the curvature form (d) $B_{12,x}$, (e) $B_{12,y}$, and (f) $B_{12,z}$.

For a given time evolution of angular velocity $\boldsymbol{\omega}(t) = [\omega_x(t),\omega_y(t),\omega_z(t)]^T$, one can compute the corresponding time evolution of quaternions by integrating the differential equations

$$\begin{pmatrix}\dot{q}_0\\ \dot{q}_1\\ \dot{q}_2\\ \dot{q}_3\end{pmatrix} = \frac{1}{2}\begin{pmatrix}q_0 & -q_1 & -q_2 & -q_3\\ q_1 & q_0 & -q_3 & q_2\\ q_2 & q_3 & q_0 & -q_1\\ q_3 & -q_2 & q_1 & q_0\end{pmatrix}\begin{pmatrix}0\\ \omega_x(t)\\ \omega_y(t)\\ \omega_z(t)\end{pmatrix}. \quad (25)$$

Based on thus computed time evolution of quaternions $[q_0(t),q_1(t),q_2(t),q_3(t)]$, one can reconstruct the evolution of the body-fixed frame $\mathsf{R}(t)$ through Eq. (24), which characterizes the geometric angle shifts.

C. Numerical implementation and results: Geometric angle shifts arising from cyclic twisting motions of a polymer chain

We numerically implement here the procedures introduced in Secs. II A and II B, and present the results for the geometric angle shifts of the five-bead polymer chain under conditions of zero total angular momentum. In the procedures above, gauge potentials $\boldsymbol{A}_\mu$ ($\mu = 1,2$) in Eq. (18) play an essential role for the computation of geometric angle shifts. Indeed, computation of the gauge potentials $\boldsymbol{A}_1$ and $\boldsymbol{A}_2$ for the five-bead polymer chain is too lengthy to be done by hand calculations. We thus used the *Mathematica* software [70] to obtain analytic expressions for the gauge potentials. While the resulted analytic expressions are also too lengthy, it is insightful to visualize the resulted gauge potentials $\boldsymbol{A}_1$ and $\boldsymbol{A}_2$ as fields in the space of dihedral angles in the following manner.

Let the three components of the gauge potentials defined in Eq. (18) be $\boldsymbol{A}_1 = (A_{1x},A_{1y},A_{1z})^T$ and $\boldsymbol{A}_2 = (A_{2x},A_{2y},A_{2z})^T$, where the subscripts 1 and 2 specify the two dihedral angles ϕ_1 and ϕ_2, whereas the subscripts x, y, and z specify the $\hat{\boldsymbol{x}}$, $\hat{\boldsymbol{y}}$, and $\hat{\boldsymbol{z}}$ axes of the body-fixed frame introduced in Sec. II A [see Fig. 1(a)]. By regrouping these components, we define two-dimensional vector fields as $\boldsymbol{A}_x \equiv (A_{1x},A_{2x})^T$, $\boldsymbol{A}_y \equiv (A_{1y},A_{2y})^T$, and $\boldsymbol{A}_z \equiv (A_{1z},A_{2z})^T$ for the sake of visualizing the gauge potentials as the fields in the space of dihedral angles. As Eq. (20) indicates, $\boldsymbol{A}_\alpha \equiv (A_{1\alpha},A_{2\alpha})^T$ ($\alpha = x,y,z$) determines the instantaneous angular velocity of the body-fixed frame about its $\hat{\boldsymbol{\alpha}}$ axis ($\hat{\boldsymbol{\alpha}} = \hat{\boldsymbol{x}},\hat{\boldsymbol{y}},\hat{\boldsymbol{z}}$) under conditions of zero total angular momentum.

Upper three panels of Fig. 2 show thus defined fields of gauge potentials (a) $\boldsymbol{A}_x$, (b) $\boldsymbol{A}_y$, and (c) $\boldsymbol{A}_z$ in the space of dihedral angles. As Eq. (23) indicates, path-ordered integral of these gauge potentials along a path in the space of dihedral angles determines the movement of the body-fixed frame under conditions of zero total angular momentum. Lower three panels of Fig. 2 show the contour plots of the curvature form

$\boldsymbol{B}_{12} \equiv (B_{12,x}, B_{12,y}, B_{12,z})^T$ in Eq. (19) for (d) $B_{12,x}$, (e) $B_{12,y}$, and (f) $B_{12,z}$. Note that these curvature forms characterize the strength and sign of "vorticity" of the fields of gauge potentials in Figs. 2(a)–2(c). One can find similar visualizations of vector fields or curvature forms in the literature of swimming [48,52] and robotics [53,54]. Intuitively, a cyclic path encircling a region of large absolute value of the curvature form can give rise to a large amount of geometric angle shift in the three-dimensional physical space. According to Figs. 2(d)–2(f), the curvature form of the gauge potentials tends to have larger magnitudes in the first and third quadrants in the space of dihedral angles as compared to the second and fourth quadrants. We thus expect that a cyclic path encircling a region in the first or the third quadrant, such as the paths in Fig. 1(b), can induce a large amount of geometric angle shift in the three-dimensional physical space.

Based on the above consideration, we examine the circular cyclic paths in the space of dihedral angles that are parametrized as

$$\phi_1(t) = \sigma + \sqrt{2}|\sigma| \cos(t + t_0), \tag{26}$$

$$\phi_2(t) = \sigma + \sqrt{2}|\sigma| \sin(t + t_0), \tag{27}$$

where t is the parameter of the path and can be regarded as time, and $t_0 = \pi/4$ or $5\pi/4$. $(\phi_1,\phi_2) = (\sigma,\sigma)$ is the center and $\sqrt{2}|\sigma|$ is the radius of the circular path. The paths in Fig. 1(b) are all of this type. For example, path (i) in Fig. 1(b) starts from the origin $[\phi_1(0),\phi_2(0)] = (0^\circ,0^\circ)$ at $t = 0$ with $t_0 = \pi/4$, and returns to the origin at $t = 2\pi$ after a left-handed cyclic revolution mainly in the third quadrant of the space of dihedral angles. At the origin, the five-bead polymer chain assumes a planar and uniformly bent conformation since the chain has no torsion, while at other points on the path, the polymer chain generally assumes "twisted" out-of-plane conformations. Thus, a cyclic revolution along the path of Eqs. (26) and (27) prescribes a *cyclic twisting motion* of the five-bead polymer chain. Here, recall that all bending angles of the polymer chain are fixed to $\theta_1 = \theta_2 = \theta_3 = 30^\circ$ and all the bond lengths are fixed to a throughout Sec. II as noted in Sec. II A. Since all the four paths in Fig. 1(b) start from the origin $[\phi_1(0),\phi_2(0)] = (0^\circ,0^\circ)$ at $t = 0$, we adopt $t_0 = \pi/4$ for paths (i) and (ii), and $t_0 = 5\pi/4$ for paths (iii) and (iv). For paths (i) and (iii), t evolves positively, while for paths (ii) and (iv), t evolves negatively.

Given a cyclic path in the space of dihedral angles [Eqs. (26) and (27)], we now implement the corresponding movements of the five-bead polymer chain in the three-dimensional physical space, i.e., time evolution of $\boldsymbol{r}_{si}$ $(i = 1,\ldots,5)$ in Eq. (7), under conditions of zero total angular momentum. This is achieved in the following steps that are based on the procedures in Secs. II A and II B:

(1) At each time t, compute the coordinates of the five beads with respect to the body-fixed frame $\boldsymbol{r}_i(t)$ $(i = 1,\ldots,5)$, using the two dihedral angles $\phi_1(t)$ and $\phi_2(t)$ and the three bending angles $\theta_1 = \theta_2 = \theta_3 = 30^\circ$ based on the procedure in Sec. II A.

(2) Compute the center of mass of the system with respect to the body-fixed frame at time t, $\boldsymbol{c}(t)$, based on Eq. (8), using the coordinates of beads $\boldsymbol{r}_i(t)$ $(i = 1,\ldots,5)$, obtained in Step 1.

(3) At each time t, compute the body-fixed frame $\mathsf{R}(t)$ by integrating Eq. (25) along the path in the space of dihedral angles $[\phi_1(t),\phi_2(t)]$, where the angular velocity components $\omega_x(t)$, $\omega_y(t)$, and $\omega_z(t)$ are determined from $\dot{\phi}_1(t)$ and $\dot{\phi}_2(t)$ via Eq. (20).

(4) After obtaining $\boldsymbol{r}_i(t)$ in Step 1, $\boldsymbol{c}(t)$ in Step 2, and $\mathsf{R}(t)$ in Step 3, transform $\boldsymbol{r}_i(t)$ into $\boldsymbol{r}_{si}(t)$ through Eq. (7) with $\boldsymbol{c}_s = \boldsymbol{0}$.

Steps 1–4 are repeated for each time step along the path in the space of dihedral angles $[\phi_1(t),\phi_2(t)]$. In Step 3, we use the leap-frog algorithm [69,71] to integrate Eq. (25). We set the initial condition for the integration of the body-fixed frame R in Step 3 as

$$q_0 = \sqrt{\frac{1}{2} + \frac{\sqrt{2}}{4}}, \quad q_1 = -\sqrt{\frac{1}{2} - \frac{\sqrt{2}}{4}}, \quad q_2 = q_3 = 0. \tag{28}$$

With this initial condition, the longitudinal axis of the five-bead polymer chain is aligned along the z_s axis of the space-fixed frame. In other words, the vector $\boldsymbol{r}_{s5} - \boldsymbol{r}_{s1}$ as well as $\boldsymbol{r}_{s4} - \boldsymbol{r}_{s2}$ is parallel to the z_s axis of the space-fixed frame at the initial configuration, where $[\phi_1(0),\phi_2(0)] = (0^\circ,0^\circ)$.

Based on the above procedures, we compute a geometric angle shift of the five-bead polymer chain in the three-dimensional physical space under conditions of zero total angular momentum. In this study, we specifically searched, on a trial and error basis, for a cyclic path in the space of dihedral angles in the form of Eqs. (26) and (27) that gives rise to a geometric angle shift by 120° about the longitudinal axis. Here, we judged the geometric angle shift by 120° in terms of the 120° change in the orientation of the third (central) bead $\boldsymbol{r}_{s3}(t)$ with respect to the center of mass. We then found that the cyclic path of Eqs. (26) and (27) with $t_0 = \pi/4, \sigma = -70.88^\circ$, and t changing from $t = 0$ to 2π, which is categorized as path (i) in Fig. 1(b), achieves this goal. Figures 3(a) and 3(b) show the snapshots of the five-bead polymer chain in the three-dimensional physical space for the three repeats of this cyclic path, i.e., from $t = 0$ to 6π. Figure 3(a) shows the "top" view of the polymer chain observed from the positive z_s axis of the space-fixed frame. Figure 3(b) shows the "side" view of the polymer chain observed from the negative y_s axis of the space-fixed frame. In each of Figs. 3(a) and 3(b), the orthogonal frame on the left represents the orientation of the space-fixed frame. The horizontal axis at the bottom of Figs. 3(a) and 3(b) represents the corresponding evolution of t. See Movie 1 in Supplemental Material [72] for the motion of the polymer chain in Fig. 3.

We confirm from Figs. 3(a) and 3(b) that every time when the system completes the cyclic twisting motion along path (i) in Fig. 1(b) and returns to the origin $(\phi_1,\phi_2) = (0^\circ,0^\circ)$, the five-bead polymer chain recovers the same planar and uniformly bent conformation. However, after this cyclic twisting motion, the orientation of the system changes by 120° in a counterclockwise manner when viewed from the positive z_s axis of the space-fixed frame. (More rigorously, our computation indicates that this angle shift by 120° is not exactly about the z_s axis but about a slightly shifted axis. However, since the difference is almost imperceptible as in Fig. 3, we ignore this difference throughout this study.) After three repeats of the cyclic twisting motion, the system recovers

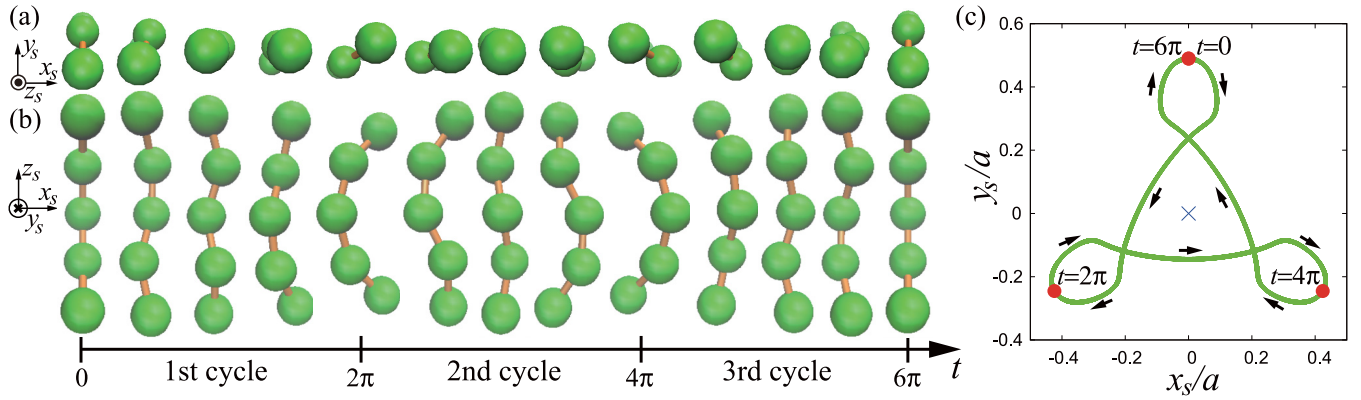

FIG. 3. (a), (b) Geometric angle shifts, i.e., somersaults, of the five-bead polymer chain through cyclic twisting motions under conditions of zero total angular momentum. The polymer chain repeats a cyclic twisting motion along the path parametrized by Eqs. (26) and (27) with $t_0 = \pi/4$ and $\sigma = -70.88^\circ$ [path (i) in Fig. 1(b)] for three times, i.e., from $t = 0$ to 6π. (a) Shows the snapshots of the system observed from the positive z_s axis of the space-fixed frame (top view) for every $\pi/2$ increment of t. (b) Shows the corresponding snapshots of the system observed from the negative y_s axis (side view). (c) Shows the projection of the corresponding trajectory of the third bead on the x_s-y_s plane (green). Arrows represent the directions of the movement. The cross symbol (blue) at the origin $(x_s, y_s) = (0,0)$ represents the center of mass of the polymer chain, which is fixed throughout the process. Three filled circles (red) represent the starting and ending points of each cyclic twisting motion, where $t = 0$, 2π, 4π, and 6π. See Movie 1 in Supplemental Material [72] for the motion of the polymer chain.

the initial orientation in the three-dimensional physical space [see the equivalence between the leftmost and rightmost snapshots in Figs. 3(a) and 3(b)]. This orientation change under conditions of zero total angular momentum is the geometric angle shift, which is of major interest in this study. We call this orientation change the *geometric somersault* in analogy with the somersault of a falling cat [13,14].

The result of Fig. 3(b) indicates that the movement of the third (central) bead of the polymer chain is confined in the narrow vicinity of the x_s-y_s plane of the space-fixed frame, where $z_s \approx 0$. We thus show in Fig. 3(c) the projection of the trajectory of the third bead (green) $\boldsymbol{r}_{s3}(t)$ onto the x_s-y_s plane of the space-fixed frame. Arrows along the trajectory represent the directions of the movement. The cross symbol (blue) at the origin $(x_s, y_s) = (0,0)$ represents the center of mass of the polymer chain, which is fixed throughout the process. Three filled circles (red) on the trajectory represent the starting and ending points of each cycle, where $t = 0$, 2π, 4π, and 6π. The trajectory in Fig. 3(c) possesses the threefold symmetry about the center of mass of the overall system, which confirms the geometric somersault by 120° for each cyclic twisting motion. We again observe that this geometric somersault by 120° is in a counterclockwise manner when viewed from the positive z_s axis. We also see that the third bead makes a small loop in the connecting part of successive cycles.

For later discussion, we divide the single cycle of the twisting motion along path (i) in Fig. 1(b) into four parts by every $\pi/2$ increment of t. In the first part, which is from $t = 0$ to $\pi/2$ in Eqs. (26) and (27), the dihedral angle ϕ_1 changes largely in the negative direction, i.e., a left-handed twist arises in ϕ_1, while the change in ϕ_2 is small. This is evident from the geometry of path (i) in Fig. 1(b), and is also confirmed in Fig. 3(b) by noting that ϕ_1 and ϕ_2 are the lower and upper dihedral angles in the snapshots of Fig. 3(b). In the second part, which is from $t = \pi/2$ to π, ϕ_2 changes largely in the negative direction, i.e., a left-handed twist arises in ϕ_2, while the change in ϕ_1 is small. In the third part, which is from $t = \pi$ to $3\pi/2$, the left-handed twist in ϕ_1 reverts back to zero, while the change in ϕ_2 is small. In the fourth part, which is from $t = 3\pi/2$ to 2π, the left-handed twist in ϕ_2 reverts back to zero, while the change in ϕ_1 is small. Thus, the cyclic twisting motion in Fig. 3 is essentially a twist propagation consisting of the sequential generation and annihilation of left-handed twists in the two dihedral angles. This type of twist propagation is of great interest not only in the rotary shafts of molecular motors, which will be discussed in Sec. III, but also in the helical motions of flagellar filaments [6–9] and in the swimming of helically shaped bacteria at low Reynolds number [73–75].

D. Relation between the directions of cyclic twisting motions and geometric angle shifts

We investigate here the directions of geometric angle shifts of the five-bead polymer chain for the four different cyclic twisting motions prescribed as paths (i)–(iv) in Fig. 1(b). Path (i) is the one that we have just scrutinized in Sec. II C. We describe path (i) as "ϕ_1(left) → ϕ_2(left)" since the two dihedral angles generate mainly left-handed twists in the order of ϕ_1 and ϕ_2, and then they revert back to zero in the same order for path (i). We then describe the resulted geometric angle shift of the polymer chain in the three-dimensional physical space as "CCW, 120°" since the system changes its orientation by 120° in the counterclockwise direction when viewed from the positive z_s axis. This is summarized in the row (i) of Table I.

Table I also summarizes the numerical results for other three cyclic paths, paths (ii)–(iv), in Fig. 1(b) with $\sigma = \pm 70.88^\circ$. For these three paths, initial configuration of the polymer chain in the three-dimensional physical space is exactly the same as that for path (i) in Sec. II C. When the system undergoes a cyclic twisting motion along path (ii) in Fig. 1(b), which follows the same path as path (i) in the reverse direction, the resulted

TABLE I. Relation between the directions of cyclic twisting motions and geometric angle shifts. The path numbers in the first column, (i)–(iv), refer to those in Fig. 1(b).

Path	Order of twists (handedness)	Geometric angle shift
(i)	ϕ_1(left) → ϕ_2(left)	CCW, 120°
(ii)	ϕ_2(left) → ϕ_1(left)	CW, 120°
(iii)	ϕ_1(right) → ϕ_2(right)	CW, 120°
(iv)	ϕ_2(right) → ϕ_1(right)	CCW, 120°

geometric angle shift is 120° in the clockwise (CW) direction when viewed from the positive z_s axis. See Movie 2 in Supplemental Material [72] for the motion of the polymer chain for path (ii). Since the two dihedral angles generate mainly left-handed twists in the order of ϕ_2 and ϕ_1, and then they revert back to zero in the same order for path (ii), we describe path (ii) as in the row (ii) of Table I. This result is understood from the time- or path-ordered product in Eq. (22) or (23). That is, along the reverse path in the space of dihedral angles, the angular velocity $\Omega(t)$ or $(-\mathsf{A}_1 d\phi_1 - \mathsf{A}_2 d\phi_2)$ in Eq. (22) or (23) arises with the opposite sign and in the reverse order.

When the system undergoes a cyclic twisting motion along path (iii) in Fig. 1(b), which is the circular path lying mainly in the first quadrant of the space of dihedral angles, the resulted geometric angle shift is 120° in the clockwise direction when viewed from the positive z_s axis. Since the two dihedral angles generate mainly right-handed twists in the order of ϕ_1 and ϕ_2, and then they revert back to zero in the same order for path (iii), we describe path (iii) as in the row (iii) of Table I. This result for path (iii), in comparison to path (i), may be understood from the consideration that the motions for paths (i) and (iii) should be mirror symmetric with respect to the y_s-z_s plane because of the opposite handedness of the dihedral angles. In addition, the opposite directionality of geometric somersaults for paths (i) and (iii) should be related to the result that the components of the curvature form plotted in Figs. 2(e) and 2(f) have opposite signs in the third and first quadrants.

When the system undergoes a cyclic twisting motion along path (iv), which follows the same path as path (iii) in the reverse direction, the resulted geometric angle shift is 120° in the counterclockwise direction when viewed from the positive z_s axis. Since the two dihedral angles generate mainly right-handed twists in the order of ϕ_2 and ϕ_1, and then they revert back to zero in the same order for path (iv), we describe path (iv) as in the row (iv) of Table I. This result for path (iv), in comparison to path (iii), can be understood similarly to the relation between paths (i) and (ii) in terms of the sign and order of angular velocity in Eq. (22) or (23).

The results in Table I are written concisely as

$$S_{\text{angle\_shift}} = -S_{\text{order}} S_{\text{handedness}}, \tag{29}$$

where $S_{\text{angle\_shift}} = +1$ for a counterclockwise geometric angle shift, and $S_{\text{angle\_shift}} = -1$ for a clockwise geometric angle shift when viewed from the positive z_s axis. S_{order} in Eq. (29) is $S_{\text{order}} = +1$ for the order of twists of $\phi_1 \to \phi_2$, and $S_{\text{order}} = -1$ for the order of twists of $\phi_2 \to \phi_1$. $S_{\text{handedness}}$ in Eq. (29) is $S_{\text{handedness}} = +1$ when ϕ_1 and ϕ_2 generate mainly right-handed twists [paths (iii) and (iv)], and $S_{\text{handedness}} = -1$ when ϕ_1 and ϕ_2 generate mainly left-handed twists [paths (i) and (ii)]. Equation (29) clarifies how the sequential order and the handedness of twists determine the direction of geometric angle shifts, and may be useful for generalization to longer polymer chains.

III. GEOMETRIC SOMERSAULTS OF A FIVE-BEAD POLYMER CHAIN DRIVEN BY EXTERNAL FORCES IN A NOISY AND VISCOUS ENVIRONMENT

In this section, we extend the model of geometric somersault of the five-bead polymer chain presented in Sec. II to a noisy and viscous environment using the Langevin dynamics. In view of the fact that biomolecules often achieve their functions through the interactions with other biomolecules or subunits, we introduce here time-dependent external forces that drive the geometric somersault of the five-bead polymer chain in a noisy and viscous environment. While the geometric somersault could be of fundamental interest in twisting and rotary motions of chainlike systems as noted at the end of Sec. II C, we argue here that the model presented in this section may serve as a prototypical and highly coarse-grained model of the rotary motion of the central shaft of F_OF_1-ATPase.

A. Internal potentials and a time-dependent external potential

The previous section (Sec. II) has focused on the kinematics of the five-bead polymer chain, where the driving forces mediating the cyclic twisting motions have not been specified. In reality, on the other hand, biomolecules usually achieve their functions through the interactions with other biomolecules or subunits. In the case of F_OF_1-ATPase, for example, the rotary motion of the central shaft is mediated by the well-coordinated interactions with other surrounding subunits [4,55,59,60,64,76,77]. This section thus incorporates a time-dependent external potential function that steers the geometric somersault of the five-bead polymer chain preventing the diffusion in the Brownian motion. Forces arising from this external potential function may be regarded as a prototypical model of the forces exerted on the central rotary shaft from the surrounding subunits in F_OF_1-ATPase as will be discussed in Sec. III E.

We first introduce internal potential functions for bonding, bending, and twisting of the five-bead polymer chain in order to model the elasticity of biomolecules. Potential function for bonding is given by

$$V_{\text{bond}} = \frac{1}{2a^2} k_{\text{bond}} \sum_{i=1}^{4} (|\boldsymbol{r}_{s(i+1)} - \boldsymbol{r}_{si}| - a)^2, \tag{30}$$

where k_{bond} is the force constant for bonding, $\boldsymbol{r}_{si}$ and $\boldsymbol{r}_{s(i+1)}$ are position vectors of ith and $(i+1)$th beads with respect to the space-fixed frame, and a is the equilibrium distance of each bond. Potential function for bending is given by

$$V_{\text{bend}} = \frac{1}{2} k_{\text{bend}} \sum_{i=1}^{3} (\theta_i - \theta_0)^2, \tag{31}$$

where k_{bend} is the force constant for bending, and θ_i is the bending angle at bead $i+1$ defined in Sec. II. The angle θ_0 is the equilibrium bending angle and is set to $\theta_0 = 30°$, which is

the same as the bending angle of the model in Sec. II. Potential function for twisting is given by

$$V_{\rm twist} = \frac{1}{2} k_{\rm twist} \sum_{i=1}^{2} \phi_i^2, \tag{32}$$

where $k_{\rm twist}$ is the force constant for twisting, and ϕ_i $(i = 1,2)$ are the two dihedral angles defined in Sec. II. Thus, the total internal potential of the polymer chain is

$$V_{\rm int} = V_{\rm bond} + V_{\rm bend} + V_{\rm twist}. \tag{33}$$

Equations (30)–(32) indicate that the equilibrium conformation of the five-bead polymer chain is the uniformly bent conformation with no twist and no stretch, where $\theta_1 = \theta_2 = \theta_3 = 30^\circ$ and $\phi_1 = \phi_2 = 0^\circ$. This equilibrium conformation is the same as the conformation in Figs. 3(a) and 3(b) at $t = 0$, 2π, 4π, and 6π.

In order to drive the movement of the five-bead polymer chain, we introduce a time-dependent external potential

$$V_{\rm ext}(\{\boldsymbol{r}_{si}\},t) = \frac{1}{2a^2} k_{\rm ext} \sum_{i=1}^{5} [\boldsymbol{r}_{si} - \tilde{\boldsymbol{r}}_{si}(t)]^2, \tag{34}$$

where $\tilde{\boldsymbol{r}}_{si}(t)$ represents a reference configuration of bead i with respect to the space-fixed frame at time t. This potential function $V_{\rm ext}(\{\boldsymbol{r}_{si}\},t)$ induces the forces that attract the bead i at $\boldsymbol{r}_{si}$ towards the reference configuration $\tilde{\boldsymbol{r}}_{si}(t)$ at each time t. The parameter $k_{\rm ext}$ determines the strength of the attractive forces. This potential function steers the five-bead polymer chain so that it follows the movement of reference configuration $\tilde{\boldsymbol{r}}_{si}(t)$ $(i = 1,\ldots,5)$. In this section, we consider the following two types of time evolutions of the reference configuration $\tilde{\boldsymbol{r}}_{si}(t)$ $(i = 1,\ldots,5)$ for comparison:

(1) In the first type, the reference configuration $\tilde{\boldsymbol{r}}_{si}(t)$ $(i = 1,\ldots,5)$ exactly follows the movement of Fig. 3 from $t = 0$ to 2π, which achieves the geometric somersault by 120° about the longitudinal axis through the cyclic twisting motion along path (i) in Fig. 1(b). We refer to the motion of the polymer chain induced by this movement of the reference configuration as the *geometric somersault*.

(2) For comparison, we also consider the second type, where the reference configuration $\tilde{\boldsymbol{r}}_{si}(t)$ $(i = 1,\ldots,5)$ undergoes a rotation about the z_s axis of the space-fixed frame by 120° with a constant angular velocity with keeping the uniformly bent equilibrium conformation determined by Eqs. (30)–(32). We refer to the motion of the polymer chain induced by this movement of the reference configuration as the *rigid-body rotation*.

For both the geometric somersault and the rigid-body rotation, we set the initial reference configuration $\tilde{\boldsymbol{r}}_{si}(0)$ $(i = 1,\ldots,5)$ to be the same. Thus, the final reference configuration is also approximately the same for the two types of time evolutions. Only the intermediate pathways of the reference configuration are largely different for the two types of time evolutions. Note that the center of mass of the reference configuration is fixed at the origin of the space-fixed frame for both the geometric somersault and the rigid-body rotation $\sum_{i=1}^{5} \tilde{\boldsymbol{r}}_{si}(t) = \boldsymbol{0}$, where we have used the fact that the five beads have the same mass. In the following, we make a comparison between the geometric somersault and the rigid-body rotation in the Langevin dynamics.

B. Langevin dynamics

We simulate the movements of the five-bead polymer chain in a noisy and viscous environment using the method of Langevin dynamics. Langevin equation for our model reads as

$$m\frac{d^2\boldsymbol{r}_{si}}{dt^2} = -\zeta\frac{d\boldsymbol{r}_{si}}{dt} - \frac{\partial V_{\rm int}}{\partial \boldsymbol{r}_{si}} - \frac{\partial V_{\rm ext}}{\partial \boldsymbol{r}_{si}} + \boldsymbol{\xi}_i(t), \tag{35}$$

where ζ is the friction coefficient and $\boldsymbol{\xi}_i(t)$ is a three-dimensional vector representing the Gaussian white noise on bead i satisfying

$$\langle \boldsymbol{\xi}_i(t) \rangle = \boldsymbol{0}, \tag{36}$$

$$\langle \boldsymbol{\xi}_i(t)\boldsymbol{\xi}_j(t') \rangle = 6\zeta k_{\rm B} T \delta_{ij}\delta(t - t'), \tag{37}$$

where $k_{\rm B}$ is the Boltzmann's constant, T is temperature, δ_{ij} is Kronecker's delta, and $\delta(t - t')$ is Dirac's delta function. After the following scaling of variables,

$$\boldsymbol{r}_{si} = a\hat{\boldsymbol{r}}_{si}, \quad t = \sqrt{\frac{ma^2}{\varepsilon}}\hat{t}, \quad \zeta = \sqrt{\frac{m\varepsilon}{a^2}}\hat{\zeta}, \tag{38}$$

$$k_{\rm B}T = \varepsilon\hat{T}, \quad V_{\rm int} = \varepsilon\hat{V}_{\rm int}, \quad V_{\rm ext} = \varepsilon\hat{V}_{\rm ext}, \tag{39}$$

where $\hat{\boldsymbol{r}}_{si}$, $\hat{t}$, $\hat{\zeta}$, $\hat{T}$ are dimensionless position vector, time, friction coefficient, temperature, and ε is the unit of energy, Eqs. (35)–(37) are put into the dimensionless forms

$$\frac{d^2\hat{\boldsymbol{r}}_{si}}{d\hat{t}^2} = -\hat{\zeta}\frac{d\hat{\boldsymbol{r}}_{si}}{d\hat{t}} - \frac{\partial \hat{V}_{\rm int}}{\partial \hat{\boldsymbol{r}}_{si}} - \frac{\partial \hat{V}_{\rm ext}}{\partial \hat{\boldsymbol{r}}_{si}} + \hat{\boldsymbol{\xi}}_i(t) \tag{40}$$

and

$$\langle \hat{\boldsymbol{\xi}}_i(\hat{t}) \rangle = \boldsymbol{0}, \tag{41}$$

$$\langle \hat{\boldsymbol{\xi}}_i(\hat{t})\hat{\boldsymbol{\xi}}_j(\hat{t}') \rangle = 6\hat{\zeta}\hat{T}\delta_{ij}\delta(\hat{t} - \hat{t}'). \tag{42}$$

We numerically solve this dimensionless Langevin equation using the velocity version of Verlet algorithm [78,79].

We now make a crude estimate of the physical parameters introduced above. We set the equilibrium bond distance between beads in Eqs. (30) and (34) to be $a = 2$ nm, which serves as the unit of length in this study. Thus, the radius of each bead of the model is assumed to be 1 nm, and the total length of the polymer chain is assumed to be about 10 nm. We also assume that the mass of each bead of the polymer chain is $m = 7$ kDa. This is based on the fact that the main subunit (γ subunit) of the central shaft of the F_OF_1-ATPase has the mass of 35 kDa [80]. We set the unit of energy to be $\varepsilon = 1000$ pNnm, and set the force constants for bonding, bending, and external driving in Eqs. (30), (31), and (34) to be $k_{\rm bond} = k_{\rm bend} = k_{\rm ext} = 20\varepsilon$. These very large force constants are essentially to fix the bonding and bending degrees of freedom and to achieve precise steering of the external forces. As for the force constant for twisting in Eq. (32), we set $k_{\rm twist} = 0.1\varepsilon = 100$ pNnm by noting that the values of twisting force constants of the central shaft of F_OF_1-ATPase are reported to be from about 10 to 1000 pNnm [64]. According to the Stokes law, the friction coefficient of water for each bead of the present model, whose radius is 1 nm, is estimated to be $\zeta = 6\pi\eta = 1.9 \times 10^{-11}$ kg s^{-1}, where $\eta = 1.0 \times 10^{-3}$ Pa s is the dynamic viscosity of water. On the other

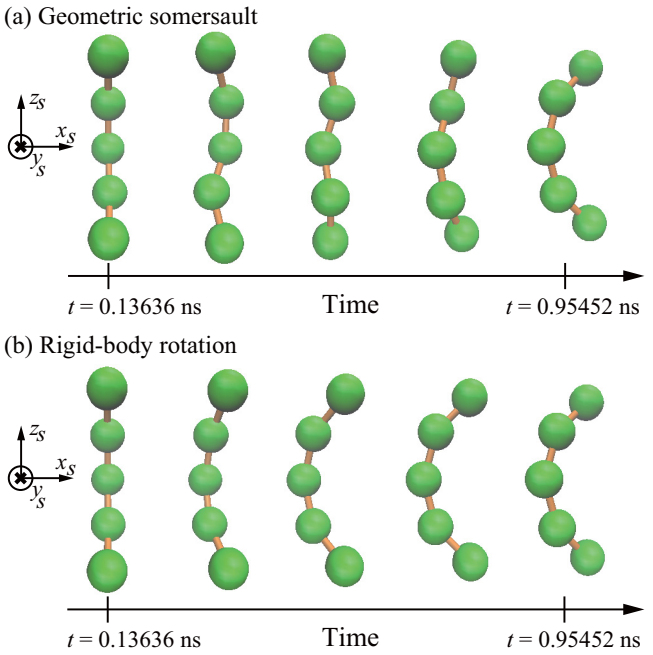

FIG. 4. Time evolutions (snapshots) of the polymer chain in the Langevin dynamics observed from the negative y_s axis of the space-fixed frame for the (a) geometric somersault and (b) rigid-body rotation. See Movies 3 and 4 in Supplemental Material [72] for the (a) geometric somersault (Movie 3) and (b) rigid-body rotation (Movie 4).

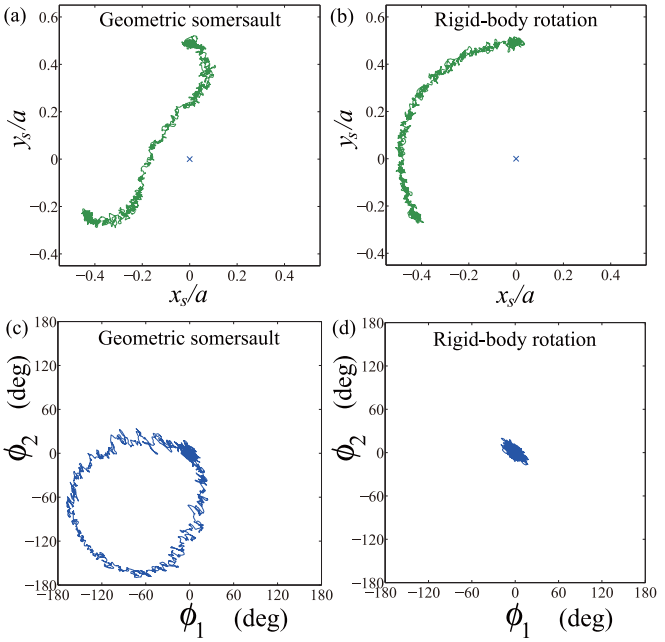

FIG. 5. Upper two panels show the projections of the trajectories of the third (central) bead of the five-bead polymer chain $\boldsymbol{r}_{s3}$ on the x-y plane in the Langevin dynamics for the (a) geometric somersault and (b) rigid-body rotation. Lower two panels show the corresponding trajectories in the space of dihedral angles in the (c) geometric somersault and (d) rigid-body rotation.

hand, the unit of friction coefficient in Eq. (38) is $\sqrt{m\varepsilon/a^2} = 1.7 \times 10^{-12}$ kg s^{-1}. Thus, we set the dimensionless friction coefficient to be $\hat{\zeta} = \zeta/\sqrt{m\varepsilon/a^2} = 11$. According to Eq. (38), the unit of time is $\sqrt{ma^2/\varepsilon} = 6.818$ ps. We set the temperature to be $T = 300$ K, which corresponds to the dimensionless temperature of $\hat{T} = k_B T/\varepsilon = 0.0041$.

C. Comparison between geometric somersault and rigid-body rotation: Angular momentum and external torque profiles

We present here the results of the Langevin dynamics of the five-bead polymer chain, and highlight the difference between the geometric somersault and the rigid-body rotation defined in Sec. III A. In the Langevin dynamics, the reference configuration $\tilde{\boldsymbol{r}}_{si}(t)$ $(i = 1, \ldots, 5)$ in Eq. (34) spends 0.818 16 ns to complete the movement of the geometric somersault or rigid-body rotation. We set a dwell time of 0.136 36 ns before and after the movement of the reference configuration $\tilde{\boldsymbol{r}}_{si}(t)$ $(i = 1, \ldots, 5)$ for both the geometric somersault and the rigid-body rotation. During the dwell time, the reference configuration $\tilde{\boldsymbol{r}}_{si}(t)$ $(i = 1, \ldots, 5)$ is fixed in the space to keep the configuration of the five-bead polymer chain near the planar uniformly bent equilibrium conformation, where $\theta_1 = \theta_2 = \theta_3 = 30^\circ$ and $\phi_1 = \phi_2 = 0^\circ$. Thus, the total time duration is $0.13636 + 0.81816 + 0.13636 = 1.09088$ ns for both the geometric somersault and rigid-body rotation. Figure 4 shows the time evolutions of the polymer chain in the Langevin dynamics observed from the negative y_s axis of the space-fixed frame for the (a) geometric somersault and (b) rigid-body rotation. See Movies 3 and 4 in Supplemental Material [72] for the motions of the polymer chain for the geometric somersault (Movie 3) and rigid-body rotation (Movie 4) in the Langevin dynamics.

Figures 5(a) and 5(b) show the projections of the trajectories of the third (central) bead of the polymer chain $\boldsymbol{r}_{s3}$ on the x_s-y_s plane for the (a) geometric somersault and (b) rigid-body rotation in the Langevin dynamics. In the case of geometric somersault in Fig. 5(a), the trajectory of the third bead essentially follows the trajectory in Fig. 3(c) for the first cycle of twisting motion with random fluctuations. In the case of rigid-body rotation in Fig. 5(b), the third bead follows the circle centered at $(x_s, y_s) = (0,0)$ with random fluctuations. In both Figs. 5(a) and 5(b), the third (central) bead changes its orientation about the z_s axis by 120°. This indicates that the movement of the reference configuration $\tilde{\boldsymbol{r}}_{si}(t)$ $(i = 1, \ldots, 5)$ has successfully guided the movement of the five-bead polymer chain through the potential of Eq. (34) for both the geometric somersault and rigid-body rotation. Because of the dwell times of 0.136 36 ns before and after the movements of the reference configuration, the beginning and ending portions of the trajectories in Figs. 5(a) and 5(b) are slightly denser and fluctuate wider than the intermediate portions.

Figures 5(c) and 5(d) show the evolutions of the two dihedral angles ϕ_1 and ϕ_2 of the five-bead polymer chain in the (c) geometric somersault and (d) rigid-body rotation corresponding to Figs. 5(a) and 5(b), respectively. In the case of geometric somersault in Fig. 5(c), the two dihedral angles ϕ_1 and ϕ_2 essentially follow the circular path (i) in Fig. 1(b) with random fluctuations, starting from and returning to the origin $(\phi_1, \phi_2) = (0^\circ, 0^\circ)$. The overall shape of the path in Fig. 5(c)

is slightly deformed from the complete circle mainly because of the internal potentials of the five-bead polymer chain and friction. In the case of rigid-body rotation in Fig. 5(d), the two dihedral angles ϕ_1 and ϕ_2 keep fluctuating in the vicinity of the origin $(\phi_1,\phi_2) = (0^\circ,0^\circ)$ throughout the Langevin dynamics. This indicates that the polymer chain has rotated by 120° like a rigid body with almost keeping its equilibrium conformation. Thus, Figs. 5(c) and 5(d) confirm that the movements of the reference configuration $\tilde{\boldsymbol{r}}_{si}(t)$ $(i = 1,\ldots,5)$ have successfully guided the prescribed geometric somersault and rigid-body rotation, respectively.

As a fundamental dynamical quantity to characterize the difference between the geometric somersault and rigid-body rotation, we investigate the time evolutions of total angular momentum of the system with respect to the space-fixed frame

$$\boldsymbol{L}_s^o = \sum_{i=1}^{5} m_i \boldsymbol{r}_{si} \times \dot{\boldsymbol{r}}_{si} \tag{43}$$

in the Langevin dynamics. This quantity $\boldsymbol{L}_s^o$ is slightly different from the total angular momentum in Eq. (13) in that the former is about the origin of the space while the latter is about the center of mass of the chain. We also investigate the time evolution of total torque of the external driving force about the origin, i.e., total external torque,

$$\boldsymbol{T}_s^o = \sum_{i=1}^{5} \boldsymbol{r}_{si} \times \left(-\frac{\partial V_{\rm ext}(\{\boldsymbol{r}_{si}\},t)}{\partial \boldsymbol{r}_{si}} \right), \tag{44}$$

where $V_{\rm ext}(\{\boldsymbol{r}_{si}\},t)$ is the time-dependent external potential in Eq. (34).

Figure 6 shows the typical time evolutions of the three components of total angular momentum of the polymer chain $\boldsymbol{L}_s^o \equiv (L_{sx}^o, L_{sy}^o, L_{sz}^o)^T$ and the three components of total torque of the external driving force $\boldsymbol{T}_s^o \equiv (T_{sx}^o, T_{sy}^o, T_{sz}^o)^T$ for the (a) geometric somersault and (b) rigid-body rotation. In each panel of Fig. 6, the two vertical broken lines at $t = 0.136\,36$ and $0.954\,52$ ns represent the beginning and ending of the movement of the reference configuration $\tilde{\boldsymbol{r}}_{si}(t)$ $(i = 1,\ldots,5)$ in Eq. (34). Since each component of total angular momentum and total torque fluctuates largely in Fig. 6, we have also plotted time- and ensemble-averaged evolution of each component with thick horizontal line (yellow) in each panel. Here, the averaging procedure is as follows. We first divide the total time duration of 1.090 88 ns into eight equal time windows of $1.090\,88/8 = 0.136\,36$ ns, where the first and the eighth time windows correspond to the dwell times, while the reference configuration of the external potential moves from the second to seventh time windows. We then average each component of Fig. 6 with respect to time in each time window. Since this time-averaged component still generally shows relatively large fluctuations, we further average this time-averaged component over 50 trajectories for each time window. In each panel of Fig. 6, the averaged value is plotted as a thick horizontal line (yellow) in each time window.

We see from Fig. 6 that all the components of $\boldsymbol{L}_s^o$ and $\boldsymbol{T}_s^o$ more or less fluctuate around zero and are averaged to zero in the case of geometric somersault in (a). In other words, the system achieves an orientation change by 120° with keeping its total angular momentum and total torque of the external driving force fluctuating around zero. This is a prominent feature of the geometric somersault in a noisy and viscous environment.

In the case of rigid-body rotation in Fig. 6(b), z_s component of the total angular momentum L_{sz}^o and that of the total torque T_{sz}^o show systematic deviations from zero, fluctuating around and averaged to nonzero values [see the two panels at the bottom of Fig. 6(b)]. On the other hand, the x_s and y_s components, L_{sx}^o, L_{sy}^o and T_{sx}^o, T_{sy}^o, more or less fluctuate around zero and are averaged to zero [see the upper four panels of Fig. 6(b)]. This is consistent with the standard picture of rigid-body rotation, which generally incurs nonzero total angular momentum and nonzero total external torque about the rotational axis, which is the z_s axis in the present case.

In both Figs. 6(a) and 6(b), the widths of fluctuations of L_{sz}^o and T_{sz}^o are smaller than those of other components. This is because the component of moment of inertia tensor of the polymer chain about the z_s axis is generally smaller than that about the x_s and y_s axis. In addition, in the case of geometric somersault in Fig. 6(a), the widths of fluctuations of L_{sz}^o and T_{sz}^o become even narrower during the course of geometric somersault. This reflects the fact that the system takes elongated conformations along the z_s axis in the course of geometric somersault as is observed in Fig. 4(a).

D. Comparison between geometric somersault and rigid-body rotation: Power profiles

In Sec. III C, we have evidenced that the five-bead polymer chain can change its orientation by 120° keeping its total angular momentum and total external torque fluctuating around zero in the case of geometric somersault. On the other hand, the rigid-body rotation incurs nonzero total angular momentum and nonzero total external torque. These results indicate that, in the geometric somersault, the work of the external driving force is mostly consumed for deformation, especially for twisting, of the polymer chain while in the rigid-body rotation, the work of the external force is mostly consumed for the pure rotation of the polymer chain. Such energetic arguments are of large interest from the viewpoint of energetics of molecular motors. We thus investigate here time evolutions of the power of the external driving forces supplied to the polymer chain

$$P = \sum_{i=1}^{5} \dot{\boldsymbol{r}}_{si} \cdot \left[-\frac{\partial V_{\rm ext}(\{\boldsymbol{r}_{si}\},t)}{\partial \boldsymbol{r}_{si}} \right], \tag{45}$$

which is a scalar quantity, for both the geometric somersault and rigid-body rotation.

Upper two panels of Fig. 7 show the time evolutions of the power defined in Eq. (45) for the (a) geometric somersault and (b) rigid-body rotation, which correspond to the same time evolutions as in Fig. 6. As these two panels indicate, the power fluctuates largely in single time evolutions. We thus average them with respect to time and ensemble of trajectories in the same manner as in Fig. 6. The lower two panels of Fig. 7 show thus averaged evolutions of the power for the (c) geometric somersault and (d) rigid-body rotation.

We see from Figs. 7(c) and 7(d) that the power profiles are quite different for the (c) geometric somersault and (d) rigid-body rotation. In the geometric somersault in Fig. 7(c), the power is positive during the first half of the evolution while

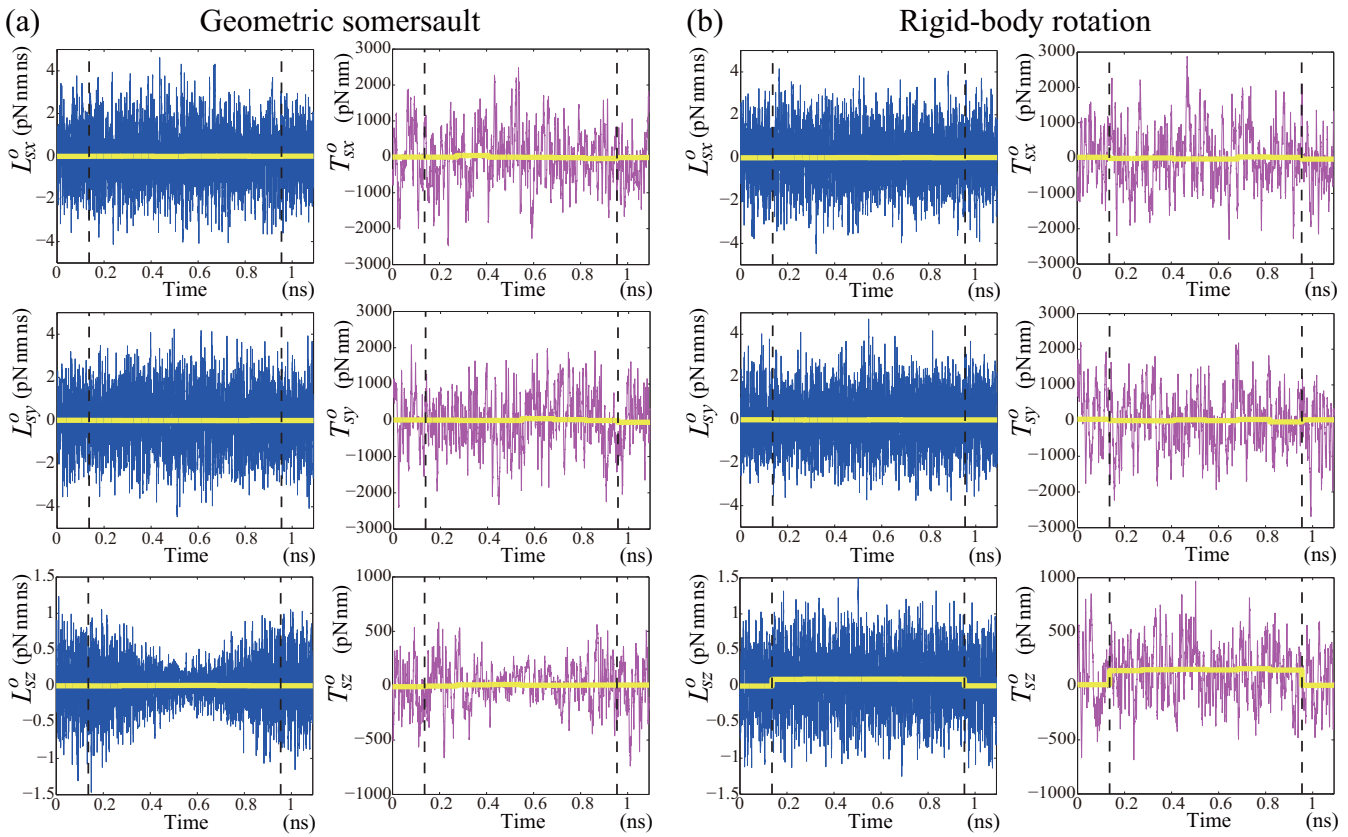

FIG. 6. Time evolutions of the three components of total angular momentum (cyan) $\boldsymbol{L}_s^o \equiv (L_{sx}^o, L_{sy}^o, L_{sz}^o)^T$ and total torque of the external driving force (magenta) $\boldsymbol{T}_s^o \equiv (T_{sx}^o, T_{sy}^o, T_{sz}^o)^T$ in the Langevin dynamics for the (a) geometric somersault and (b) rigid-body rotation. In each panel, two vertical broken lines at $t = 0.136\,36$ and $0.954\,52$ ns represent the beginning and ending of the movements of the reference configuration $\tilde{\boldsymbol{r}}_{si}(t)$ in Eq. (34). Thick horizontal line (yellow) in each panel represents time- and ensemble-averaged evolution of each quantity. Notice that all the time evolutions in (a) more or less fluctuate around zero and are averaged to zero, while the time evolutions of L_{sz}^o and T_{sz}^o at the bottom of (b) show systematic deviations from zero during the movement of the reference configuration.

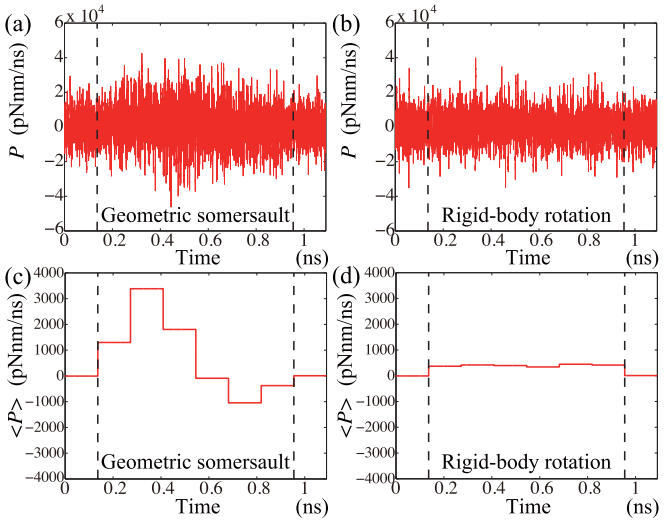

FIG. 7. Upper two panels show time evolutions of the power of the external driving force P defined in Eq. (45), in the Langevin dynamics for the (a) geometric somersault and (b) rigid-body rotation. Lower two panels show time- and ensemble-averaged time evolutions of the power for the (c) geometric somersault and (d) rigid-body rotation.

it is negative during the last half of the evolution. The positive power originates mainly from the work of the external driving forces to generate twists in the two dihedral angles against the twisting potential in Eq. (32) from about $(\phi_1,\phi_2) = (0^\circ,0^\circ)$ to about $(\phi_1,\phi_2) = (-142^\circ,-142^\circ)$ along the first half of the trajectory in Fig. 5(c). The positive power also reflects the work of the external driving forces to move the polymer chain against friction. On the other hand, the negative power in Fig. 7(c) arises when the dihedral angles of the polymer chain release the accumulated twisting energy from about $(\phi_1,\phi_2) = (-142^\circ, -142^\circ)$ to about $(\phi_1,\phi_2) = (0^\circ,0^\circ)$ along the last half of the trajectory in Fig. 5(c). This negative power indicates that the polymer chain relaxes the twisting strain almost spontaneously without much relying on the steering of the external driving force. To summarize the entire process of Fig. 7(c), the external driving force first supplies energy to the polymer chain, and the polymer chain stores this energy mainly in the form of the twisting potential energy, and finally the polymer chain releases this energy to outside actively. By integrating the averaged power with time for the first half of Fig. 7(c), we see that the energy supplied by the external driving force to the polymer chain is about 880 pNnm. On the other hand, by integrating the averaged power with time for the last half of Fig. 7(c), we see that the energy released by the polymer chain

to outside is about −210 pNnm. Thus, the total dissipated energy in the geometric somersault is estimated to be about 670 pNnm.

In the case of rigid-body rotation in Fig. 7(d), the averaged power is always positive and is almost constant during the movement of the reference configuration. This indicates that the external driving force needs to supply energy continuously in order to rotate the polymer chain with an almost constant angular velocity against friction. By integrating the averaged power in Fig. 7(d) with time for the whole time span, we see that the total energy supplied by the external driving force is about 320 pNnm. This amount of energy is smaller than the total supplied energy of 880 pNnm in the geometric somersault in Fig. 7(c) mainly because the external driving forces do not need to supply energy to deform the polymer chain in the case of rigid-body rotation.

In both the geometric somersault and rigid-body rotation, the velocity of moving the beads of the polymer chain is a decisive factor to determine the power and total supplied energy. Since friction is proportional to the velocity of beads, one can generally reduce the power and total supplied energy of the external driving forces by reducing the velocity of reference configuration and spending more time for the same amount of angle shift. Moreover, in the case of geometric somersault, the polymer chain can release more energy to outside if the movement of the reference configuration is slower. This is because when the movement of the reference configuration is slower, the polymer chain relaxes its twisting strain more spontaneously without much relying on the steering of the external driving forces. On the other hand, when the movement of the reference configuration is fast and dominates the movement of the polymer chain, relaxation of the twisting strain of the polymer chain becomes passive and cannot give much energy to outside. Thus, one can generally expect a higher ratio of released energy to supplied energy, i.e., a higher efficiency, by moving the reference configuration more slowly.

E. Discussion: Implications for the rotary motion of the central shaft of F_OF_1-ATPase

We finally discuss implications of the geometric somersault of the five-bead polymer chain studied in this study for the rotary motion of the central shaft of F_OF_1-ATPase. While the standard picture for the rotary motion of the central shaft of F_OF_1-ATPase may be more or less like the rigid-body rotation studied in Figs. 4(b), 5(b), 5(d), 6(b), 7(b) and 7(d), we argue here that the actual motion of the central shaft could be rather like the geometric somersault studied in Figs. 3, 4(a), 5(a), 5(c), 6(a), 7(a) and 7(c).

Figure 8(a) shows a schematic illustration of F_OF_1-ATPase. The F_O domain of this molecular motor is embedded in the membrane, while the F_1 domain is protruded from the membrane. These two domains are connected with the central rotary shaft, the so-called "central rotor," which consists of γ, ε, and c subunits [55,63], as colored in green in Fig. 8(a). This central rotary shaft is surrounded by the $\alpha_3\beta_3$ complex in the F_1 domain. The peripheral part consisting of a, b, and δ is considered to serve as a static "stator stalk" preventing corotation of the $\alpha_3\beta_3$ complex with the central rotary shaft [63,81]. The F_O and F_1 domains drive rotary

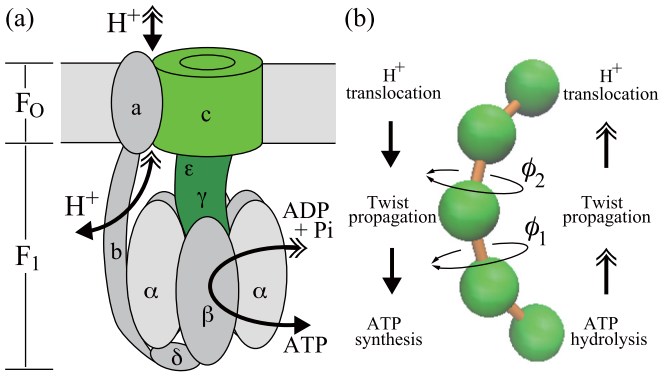

FIG. 8. (a) Schematic illustration of F_OF_1-ATPase, where the colored subunits (green) γ, ε, and c constitute the central rotary shaft, the so-called "central rotor" [55,63]. Different arrowheads correspond to different functions, i.e., ATP hydrolysis and ATP synthesis. (b) The present model of the five-bead polymer chain may coarsely serve as a prototypical model of the central rotary shaft of F_OF_1-ATPase.

motions of the central shaft in opposite directions, which are associated with opposite functions: Hydrolysis of ATP in the F_1 domain induces a stepwise rotary motion of the central shaft by 120° in a counterclockwise manner (when observed from the membrane side), which is supposed to transmit energy to the F_O domain to translocate protons across the membrane [55]. The actual stepwise rotary motion by 120° is known to consist of two substeps [5,56,57]. On the other hand, proton-motive force at F_O domain due to proton translocation across the membrane induces a rotary motion of the central shaft in a clockwise manner (when observed from the membrane side) [58–60], which is supposed to transmit energy to the F_1 domain to synthesize ATP [55,61].

The clockwise and counterclockwise rotary motions of the central shaft of F_OF_1-ATPase may be modeled coarsely by the geometric somersault of the five-bead polymer chain of this study as follows after disregarding the details of structures and substep motions. We first suppose that the dihedral angle ϕ_1 of the present model of the polymer chain roughly corresponds to the F_1 side of the central shaft, while the dihedral angle ϕ_2 roughly corresponds to the F_O side of the central shaft [see Fig. 8(b)]. In the geometric somersaults in Figs. 3, 4(a), 5(a), 5(c), 6(a), 7(a), and 7(c), which all stem from the cyclic twisting motion of path (i) in Fig. 1(b), the dihedral angles generate mainly left-handed twists in the sequential order of ϕ_1 and ϕ_2, and then they revert back to zero in the same order. After this cyclic twisting motion, the polymer chain changes its orientation by 120° in a counterclockwise manner when observed from above in Fig. 8(b). This type of geometric somersault could take place in the central shaft of the F_OF_1-ATPase upon ATP hydrolysis in the following scenario.

In ATP hydrolysis, the F_1 portion of the central shaft receives driving forces from the surrounding subunits α and β, where ATP hydrolysis actually takes place [see Fig. 8(a)] [4,64,76,77]. These driving forces might induce a left-handed twist in the F_1 portion of the central shaft first. Such left-handed twist in the F_1 portion may propagate to the F_O portion through the internal elastic coupling and induce a left-handed twist in the F_O portion of the central shaft as well. Then, the induced left-handed twists in the F_1 and F_O

portions of the central shaft may finally relax in this order. In this manner, the central shaft of the F_OF_1-ATPase may complete a cyclic twisting motion like path (i) in Fig. 1(b) upon ATP hydrolysis. If this is the case, the central shaft of the F_OF_1-ATPase can undergo a geometric somersault by 120° in a counterclockwise manner (when observed from the membrane side) as Figs. 3, 4(a), 5(a) and 5(c) have indicated.

We can also argue that the clockwise angle shift of the central shaft of the F_OF_1-ATPase in ATP synthesis might be like the geometric somersault of the present polymer chain model induced by the cyclic twisting motion of path (ii) in Fig. 1(b), which is the reverse of path (i), as follows. In ATP synthesis, the F_O portion of the central shaft receives driving forces first since the proton translocation takes place in the F_O domain [see Fig. 8(a)] [55,59,60]. These driving forces might induce a left-handed twist in the F_O portion of the central shaft first. Such left-handed twist in the F_O portion may propagate to the F_1 portion through the internal elastic coupling and induce a left-handed twist in the F_1 portion of the central shaft as well. Then, the induced left-handed twists in the F_O and F_1 portions of the central shaft may finally relax in this order. In this manner, the central shaft of the F_OF_1-ATPase may complete a cyclic twisting motion like path (ii) in Fig. 1(b) upon ATP synthesis. If this is the case, the central shaft of the F_OF_1-ATPase can undergo a geometric somersault in a clockwise manner (when observed from the membrane side) as the row (ii) of Table I has indicated.

It should be noted that, in the above scenarios for ATP hydrolysis and synthesis, there are mainly two basic assumptions. The first is the propagation of twists in the central shaft from F_1 to F_O for ATP hydrolysis and from F_O to F_1 for ATP synthesis. The present model of five-bead polymer chain does not possess the internal mechanism for such propagation of twists between the two dihedral angles ϕ_1 and ϕ_2. That is, in the geometric somersault in vacuum in Fig. 3, we have just assumed the prescribed changes in ϕ_1 and ϕ_2, and have not specified the driving forces. In the geometric somersault in the Langevin dynamics in Figs. 4(a), 5(a), 5(c), 6(a), 7(a), and 7(c), on the other hand, the external driving forces have completely guided the twisting motion. Thus, in order for the present model to be more consistent with the picture of elastic power transmission suggested by the mismatch of the rotational symmetries of F_O and F_1 domains [55,60,62–64], it would be necessary to introduce an elastic coupling between ϕ_1 and ϕ_2, which mediates the propagation of twists between these two dihedral angles. Such internal mechanism for twist propagation would reduce the total amount of mechanical work of the external driving forces in Fig. 7(c). Given the fact that the central shaft of F_OF_1-ATPase consists of a long coiled coil [2] and is torsionally compliant [55,63,64], the present assumption of twist propagation seems to be possible. Once the mechanism for twist propagation is established, the present model of geometric somersault may provide a basis for the picture that local interactions between the central shaft and the surrounding subunits [76,77] can induce the global angle shift in the narrow cavity of the molecular motor.

The second basic assumption in the above scenarios for ATP hydrolysis and synthesis is the left-handedness of induced twists in both F_1 and F_O portions of the central shaft. The left-handedness of twists seems to be necessary in order for the present model of geometric somersault to be consistent with reality: If the two dihedral angles were to generate right-handed twists in the order of ϕ_1 and ϕ_2, and then revert back to zero in the same order upon ATP hydrolysis, the central shaft would undergo a geometric somersault in a clockwise manner according to the row (iii) of Table I, which is inconsistent with the actual counterclockwise angle shift of the central shaft [3–5]. Similarly, if the two dihedral angles were to generate right-handed twists in the order of ϕ_2 and ϕ_1, and then revert back to zero in the same order upon ATP synthesis, the central shaft would undergo a geometric somersault in a counterclockwise manner according to the row (iv) of Table I, which is inconsistent with the actual clockwise angle shift of the central shaft [55,58–60]. Thus, in Table I, the rows (i) and (ii) give the most plausible models for the rotary motions of the central shaft for ATP hydrolysis and synthesis, respectively.

Finally, we note another motivation for considering the geometric somersault of the central shaft in the function of F_OF_1-ATPase from the viewpoint of the transfer (balance) of angular momentum and torque. If the central shaft were to possess nonzero total angular momentum due to nonzero total torque supplied by the surrounding subunits as in the rigid-body rotation, the surrounding subunits would inevitably tend to rotate as a whole in the opposite direction as a result of the reaction torque. For example, in ATP hydrolysis, if the $\alpha_3\beta_3$ complex were to apply nonzero total torque on the central shaft and the central shaft were to rotate as a rigid body, the $\alpha_3\beta_3$ complex would tend to rotate in the opposite direction due to the reaction torque. If this is the case, the "stator stalk" domain, a, b, and δ in Fig. 8(a), would be subject to a strong mechanical load to prevent the corotation of the $\alpha_3\beta_3$ complex, which could lead to a dissipation of energy. On the other hand, if the central shaft undergoes a geometric somersault without causing total angular momentum or total torque, the $\alpha_3\beta_3$ complex would receive no reaction torque and the mechanical load on the "stator stalk" domain could be small, preventing energy dissipation.

IV. CONCLUDING REMARKS

This study has explored the significance of geometric angle shifts, which we have called geometric somersaults, arising from cyclic twisting motions of a polymer chain both in vacuum and in a noisy and viscous environment. A five-bead polymer chain has served as a simple model of a molecular shaft. We have demonstrated that this polymer chain can undergo a geometric somersault about its longitudinal axis largely, e.g., 120°, under conditions of zero total angular momentum in vacuum by changing the two dihedral angles in a cyclic manner. We have then extended this model to a noisy and viscous environment, where the polymer chain is driven by external driving forces and achieves an orientation change keeping its total angular momentum and total torque of the external driving forces fluctuating around zero.

As an application, we have argued that the geometric somersault of the five-bead polymer chain by 120° may serve as a prototypical model for the rotary motion of the central shaft of ATP synthase (F_OF_1-ATPase). As Fig. 6 has indicated, the model of geometric somersault has been in clear contrast to the standard picture for the rotary motion

of the central shaft of F_OF_1-ATPase, which is more or less like a "rigid-body rotation" incurring nonzero total angular momentum and nonzero total torque of external driving forces. The model of geometric somersault has implied, in Fig. 7(c), a preliminary mechanism for elastic power transmission, where the external driving forces first supply energy to the central shaft, and then the central shaft stores this energy mainly in the form of twisting potential energy, and finally releases this energy to outside spontaneously. We have noted that at least two fundamental assumptions need to be tested in order for the present model of geometric somersault to be acceptable: the first has been the propagation of twists through the central shaft, and the second has been the left-handedness of twists arising and propagating in the central shaft. Finer scale analyses at the level of tertiary or secondary structures of F_OF_1-ATPase would judge these assumptions.

This study has aimed at developing a minimal model of a polymer chain that can achieve a geometric somersault by 120° about its longitudinal axis. Our initial study on a four-bead polymer chain, which has only one dihedral angle and two bending angles, indicated a difficulty in achieving a geometric somersault by 120° about its longitudinal axis. Thus, the five-bead polymer chain of this study, having two dihedral angles, seems to be a minimal model that achieves the goal. This result suggests that the central shaft of F_OF_1-ATPase must have at least two torsionally compliant parts in order for the geometric somersault to take place in its actual function. Using the two dihedral angles of the five-bead polymer chain, it is not difficult to design geometric somersaults by, e.g., 80° and 40°, which may serve as the models for the substep rotary motions of the central shaft of F_OF_1-ATPase [5,56,57]. In reality, however, the central shaft of F_OF_1-ATPase may have more torsional degrees of freedom. If this is the case, the amount of twist of each torsional degree of freedom can be smaller than those of the five-bead polymer chain to achieve a geometric somersault by 120°. Moreover, a model with more torsional degrees of freedom can achieve wider varieties of geometric somersaults, which may be useful to model the rotary shaft of F_OF_1-ATPase more finely.

The total amount of supplied energy in the geometric somersault of the five-bead polymer chain, about 880 pNnm according to Fig. 7(c), has been higher than that in the rigid-body rotation, about 320 pNnm according to Fig. 7(d). This does not necessarily mean that the rigid-body rotation is energetically more advantageous than the geometric somersault. In the narrow cavity of F_OF_1-ATPase, a rigid-body rotation of the central shaft may face steric hindrances as was pointed out in Ref. [65], which may incur an additional energy. On the other hand, a motion like the geometric somersault, which consists of local twists and relaxations of the shaft, may be more suitable in the narrow cavity of F_OF_1-ATPase.

In order for the model of geometric somersault to be more realistic, it is also important to reduce the total amount of supplied energy up to the experimentally estimated value of 80 pNnm [11], which is known to be almost the same as the free energy of hydrolysis of one ATP. There are several ways to reduce the required energy of the present model. For one thing, reducing the force constant for twisting, k_{twist} in Eq. (32), will reduce the supplied energy to achieve the geometric somersault. For another, reducing the velocity of moving the beads will also reduce the supplied energy. Finally, as discussed in Sec. III E, introducing an elastic coupling between the two dihedral angles would reduce the energy supplied by the external driving forces. In a more realistic model, external driving forces first generate a twist in one side of the shaft, then this twist propagates to the other side of the shaft through the internal elastic coupling, and the shaft finally releases energy or achieves a mechanical work when these twists relax. In order to build such a model, fine tuning of torsional rigidity, moving velocities, and elastic coupling of the shaft would be important. The relation among molecular flexibility, moving velocities, and motor efficiency is of crucial importance for the understanding of the dynamics of molecular motors [9,82,83].

Geometric somersaults of this study may imply a rather universal significance of the kinematic coupling between twisting motions and rotations in chainlike systems. That is, a chainlike system can easily change its orientation just by propagating and relaxing a twist from one side to the other without using total angular momentum or external torque. This type of twist propagation and the resulted geometric somersaults may be of fundamental significance among biological systems, given the fact that biomolecules are typically helical, i.e., intrinsically twisted. Exploring the roles of geometric somersaults in the functions of flagella [6–9] as well as in the swimming of helically shaped bacteria [74,75] is of significant interest for future studies.

ACKNOWLEDGMENTS

The authors would like to thank K. Yoshikawa, W. S. Koon, and C. Hartmann for stimulating discussions and encouragement. Graphics and movies of the polymer chain in this study have been created by VMD [84]. This study has been partially supported by JSPS (Japan) Grant-in-Aid No. 26800207.

[1] P. D. Boyer, Biochim. Biophys. Acta **1140**, 215 (1993).
[2] J. P. Abrahams, A. G. W. Leslie, R. Lutter, and J. E. Walker, Nature (London) **370**, 621 (1994).
[3] H. Noji, R. Yasuda, M. Yoshida, and K. Kinosita, Nature (London) **386**, 299 (1997).
[4] H. Wang and G. Oster, Nature (London) **396**, 279 (1998).
[5] R. Yasuda, H. Noji, M. Yoshida, K. Kinosita, and H. Itoh, Nature (London) **410**, 898 (2001).
[6] H. C. Berg and R. A. Anderson, Nature (London) **245**, 380 (1973).
[7] H. C. Berg, Annu. Rev. Biochem. **72**, 19 (2003).
[8] Y. Sowa, A. D. Rowe, M. C. Leake, T. Yakushi, M. Homma, A. Ishijima, and R. M. Berry, Nature (London) **437**, 916 (2005).
[9] J. Xing, F. Bai, R. Berry, and G. Oster, Proc. Natl. Acad. Sci. USA **103**, 1260 (2006).
[10] F. Oosawa, Genes Cells **5**, 9 (2000).

[11] R. Yasuda, H. Noji, K. Kinosita, and M. Yoshida, Cell **93**, 1117 (1998).
[12] M. Takano, T. P. Terada, and M. Sasai, Proc. Natl. Acad. Sci. USA **107**, 7769 (2010).
[13] T. R. Kane and M. P. Scher, Int. J. Solids Struct. **5**, 663 (1969).
[14] C. Frohlich, Sci. Am. **242**, 154 (1980).
[15] J. E. B. Wilson, J. C. Decius, and P. C. Cross, *Molecular Vibrations: The Theory of Infrared and Raman Vibrational Spectra* (Dover, New York, 1980).
[16] C. Eckart, Phys. Rev. **47**, 552 (1935).
[17] J. D. Louck and H. W. Galbraith, Rev. Mod. Phys. **48**, 69 (1976).
[18] K. N. Kudin and A. Y. Dymarsky, J. Chem. Phys. **122**, 224105 (2005).
[19] M. Martinez, M.-P. Gaigeot, D. Borgis, and R. Vuilleumier, J. Chem. Phys. **125**, 144106 (2006).
[20] R. J. Hinde and R. S. Berry, J. Chem. Phys. **99**, 2942 (1993).
[21] A. Kitao and N. Gō, J. Comput. Chem. **12**, 359 (1991).
[22] A. Kitao, S. Hayward, and N. Go, Biophys. Chem. **52**, 107 (1994).
[23] P. H. Nguyen and G. Stock, J. Chem. Phys. **119**, 11350 (2003).
[24] W. H. Miller, N. C. Handy, and J. E. Adams, J. Chem. Phys. **72**, 99 (1980).
[25] M. Page and J. W. McIver, J. Chem. Phys. **88**, 922 (1988).
[26] D. J. Tobias and C. L. Brooks, J. Chem. Phys. **89**, 5115 (1988).
[27] R. Elber, J. Chem. Phys. **93**, 4312 (1990).
[28] E. Neria, S. Fischer, and M. Karplus, J. Chem. Phys. **105**, 1902 (1996).
[29] A. Kitao, F. Hirata, and N. Go, Chem. Phys. **158**, 447 (1991).
[30] F. Sittel, A. Jain, and G. Stock, J. Chem. Phys. **141**, 014111 (2014).
[31] M. Kummer, Indiana Univ. Math. J. **30**, 281 (1981).
[32] R. Montgomery, J. Marsden, and T. Ratiu, Contemp. Math. **28**, 101 (1984).
[33] R. Montgomery, in *Dynamics and Control of Mechanical Systems: The Falling Cat and Related Problems*, Fields Institute Communications, Vol. 1, edited by M. J. Enos (American Mathematical Society, Providence, 1993), pp. 193–218.
[34] J. E. Marsden and T. S. Ratiu, *Introduction to Mechanics and Symmetry* (Springer, New York, 1999).
[35] A. M. Bloch, *Nonholonomic Mechanics and Control* (Springer, New York, 2003).
[36] A. Guichardet, Ann. Inst. Henri Poincaré Phys. Theor. **40**, 329 (1984).
[37] A. Tachibana and T. Iwai, Phys. Rev. A **33**, 2262 (1986).
[38] T. Iwai, Ann. Inst. Henri Poincaré Phys. Theor. **47**, 199 (1987).
[39] R. G. Littlejohn and M. Reinsch, Rev. Mod. Phys. **69**, 213 (1997).
[40] T. Yanao and K. Takatsuka, Phys. Rev. A **68**, 032714 (2003).
[41] T. Yanao and K. Takatsuka, J. Chem. Phys. **120**, 8924 (2004).
[42] T. Yanao, W. S. Koon, J. E. Marsden, and I. G. Kevrekidis, J. Chem. Phys. **126**, 124102 (2007).
[43] T. Yanao, W. S. Koon, and J. E. Marsden, J. Chem. Phys. **130**, 144111 (2009).
[44] Y. Oka, T. Yanao, and W. S. Koon, J. Chem. Phys. **142**, 134105 (2015).
[45] C. Hartmann and T. Yanao, Mol. Phys. **111**, 3534 (2013).
[46] A. Shapere and F. Wilczek, Phys. Rev. Lett. **58**, 2051 (1987).
[47] J. E. Avron, O. Gat, and O. Kenneth, Phys. Rev. Lett. **93**, 186001 (2004).
[48] J. E. Avron and O. Raz, New J. Phys. **10**, 063016 (2008).
[49] J. Wisdom, Science **299**, 1865 (2003).
[50] S. D. Kelly and R. M. Murray, J. Robotic Syst. **12**, 417 (1995).
[51] J. Ostrowski and J. Burdick, Int. J. Robotic Res. **17**, 683 (1998).
[52] J. B. Melli, C. W. Rowley, and D. S. Rufat, SIAM J. Appl. Dyn. Syst. **5**, 650 (2006).
[53] R. L. Hatton and H. Choset, Int. J. Robotic Res. **30**, 988 (2011).
[54] R. L. Hatton, Y. Ding, H. Choset, and D. I. Goldman, Phys. Rev. Lett. **110**, 078101 (2013).
[55] W. Junge, H. Sielaff, and S. Engelbrecht, Nature (London) **459**, 364 (2009).
[56] K. Shimabukuro, R. Yasuda, E. Muneyuki, K. Y. Hara, K. Kinosita, and M. Yoshida, Proc. Natl. Acad. Sci. USA **100**, 14731 (2003).
[57] C.-B. Li, H. Ueno, R. Watanabe, H. Noji, and T. Komatsuzaki, Nat. Commun. **6**, 10223 (2015).
[58] D. Stock, A. G. W. Leslie, and J. E. Walker, Science **286**, 1700 (1999).
[59] A. Aksimentiev, I. A. Balabin, R. H. Fillingame, and K. Schulten, Biophys. J. **86**, 1332 (2004).
[60] M. G. Düser, N. Zarrabi, D. J. Cipriano, S. Ernst, G. D. Glick, S. D. Dunn, and M. Börsch, EMBO J. **28**, 2689 (2009).
[61] H. Itoh, A. Takahashi, K. Adachi, H. Noji, R. Yasuda, M. Yoshida, and K. Kinosita, Nature (London) **427**, 465 (2004).
[62] H. Sielaff, H. Rennekamp, A. Wächter, H. Xie, F. Hilbers, K. Feldbauer, S. D. Dunn, S. Engelbrecht, and W. Junge, Proc. Natl. Acad. Sci. USA **105**, 17760 (2008).
[63] A. Wächter, Y. Bi, S. D. Dunn, B. D. Cain, H. Sielaff, F. Wintermann, S. Engelbrecht, and W. Junge, Proc. Natl. Acad. Sci. USA **108**, 3924 (2011).
[64] J. Czub and H. Grubmüller, Proc. Natl. Acad. Sci. USA **108**, 7408 (2011).
[65] C. Kutzner, J. Czub, and H. Grubmüler, J. Chem. Theory Comput. **7**, 1381 (2011).
[66] A. Patriciu, G. S. Chirikjian, and R. V. Pappu, J. Chem. Phys. **121**, 12708 (2004).
[67] T. Yanao and K. Yoshikawa, Phys. Rev. E **89**, 062713 (2014).
[68] V. Aquilanti and S. Cavalli, J. Chem. Phys. **85**, 1355 (1986).
[69] M. P. Allen and D. J. Tildesley, *Computer Simulation of Liquids* (Oxford University Press, New York, 1989).
[70] Wolfram Research, Inc., *Mathematica*, Version 9.0 (Champaign, IL, 2013).
[71] D. Fincham, CCP5 Information Quarterly **2**, 6 (1981).
[72] See Supplemental Material at http://link.aps.org/supplemental/10.1103/PhysRevE.95.012409 for movies of geometric somersaults of the five-bead polymer chain both in vacuum and in a noisy and viscous environment.
[73] E. M. Purcell, Am. J. Phys. **45**, 3 (1977).
[74] J. W. Shaevitz, J. Y. Lee, and D. A. Fletcher, Cell **122**, 941 (2005).
[75] H. Wada and R. R. Netz, Phys. Rev. E **80**, 021921 (2009).
[76] N. Koga and S. Takada, Proc. Natl. Acad. Sci. USA **103**, 5367 (2006).
[77] J. Pu and M. Karplus, Proc. Natl. Acad. Sci. USA **105**, 1192 (2008).

[78] Z. Guo and D. Thirumalai, Biopolymers **36**, 83 (1995).
[79] Z. Guo and D. Thirumalai, J. Mol. Biol. **263**, 323 (1996).
[80] S. Neumann, U. Matthey, G. Kaim, and P. Dimroth, J. Bacteriol. **180**, 3312 (1998).
[81] J. Weber, Trends Biochem. Sci. **32**, 53 (2007).
[82] H. Wang and G. Oster, Europhys. Lett. **57**, 134 (2002).
[83] H. Wang and H. Zhou, Abstract Appl. Anal. **2008**, 241736 (2008).
[84] W. Humphrey, A. Dalke, and K. Schulten, J. Mol. Graphics **14**, 33 (1996).